A Delay-Tolerant Asynchronous Two-Way-Relay System over Doubly-Selective Fading Channels

Ahmad Salim, *Student Member, IEEE*, and Tolga M. Duman, *Fellow, IEEE*

***Abstract*—We consider design of asynchronous orthogonal frequency division multiplexing (OFDM) based diamond two-way-relay (DTWR) systems in a time-varying frequency-selective (doubly-selective) fading channel. In a DTWR system, two users exchange their messages with the help of two relays. Most of the existing works on asynchronous DTWR systems assume only small relative propagation delays between the received signals at each node that do not exceed the length of the cyclic-prefix (CP). However, in certain practical communication systems, significant differences in delays may take place, and hence existing solutions requiring excessively long CPs may be highly inefficient. In this paper, we propose a delay-independent CP insertion mechanism in which the CP length depends only on the number of subcarriers and the maximum delay spread of the corresponding channels. We also propose a symbol detection algorithm that is able to tolerate very long relative delays, that even exceed the length of the OFDM block itself, without a large increase in complexity. The proposed system is shown to significantly outperform other alternatives in the literature through a number of specific examples.**

***Index Terms*—Two-way relay channels, underwater acoustic communications, synchronization, OFDM.**

I. Introduction

COOPERATIVE communications is an effective technique that uses relay nodes to provide various performance advantages including virtual spatial diversity and coverage extension. Advancements in this field led to the introduction of two-way relay (TWR) systems in which two source nodes are able to simultaneously communicate with each other through the aid of a relay node. Recently, TWR systems have received increased attention as not only they can overcome coverage problems, but also they provide a means of two-way communication. These advantages are even possible without requiring any additional resources compared to single-way relay systems by exploiting the inherent superimposition nature of electromagnetic waves in cooperative wireless networks. This, however, comes at the price of requiring strict synchronization between the communicating users, and while this is attainable in many communication systems, it is not in others. One such application that we consider in this paper is underwater acoustic (UWA) communications in which significant relative delays are experienced between signals originating from different nodes due to the low speed of sound propagation.

The UWA channel is considered one of the harshest communication media nowadays [1]. Excessively large propagation delays, time-and frequency selectivity are some of the major impairments in UWA channels. Because of the low speed of sound in water ($\approx$1500 m/s), differences in the propagation distance in the range of hundreds of meters result in large relative delays in the range of hundreds of milliseconds. Therefore, having an accurately synchronized DTWR system can be difficult and novel schemes are required to face asynchronism, or even better, to harness it to our advantage.

Many schemes have been proposed in the literature to solve the asynchronism problem in two-way relaying for both single-carrier and multi-carrier communication systems. Among them, our focus in this paper is on multi-carrier systems. To address the asynchronism caused by having simultaneously received signals experiencing different delay spreads, Lu *et al.* propose an OFDM-based TWR scheme in [2]. By using OFDM, the relative time dispersion caused by the multipath channel is reduced, and as long as the maximum of the delay spreads experienced is within the cyclic-prefix (CP), the effect disappears in the frequency domain. In [3], the authors propose a scheme based on sphere decoding to mitigate the effects of time misalignment for an OFDM-modulated channel-coded TWR system over a frequency-selective fading channel. Two precoding-based schemes are proposed in [4] based on channel inversion.

In [5], the authors propose a scheme that jointly mitigates synchronization errors, provides full spatial diversity and has the property of fast maximum likelihood decoding. The scheme is based on inserting an appropriate CP and performing simple operations at the relay such as conjugation and time-reversal. Besides overcoming the asynchronism, the scheme in [5] results in an equivalent orthogonal space time block code (OSTBC) structure or a quasi-OSTBC structure on each subcarrier at each user, which simplifies decoding of the partner's message. [6] proposes an OFDM-based scheme for asynchronous TWR systems that maximizes the worst signal-to-noise ratio (SNR)

Manuscript received August 1, 2014; revised November 13, 2014 and February 5, 2015; accepted March 4, 2015. Date of publication March 18, 2015; date of current version July 8, 2015. Part of this work was presented at the International Conference on Computing, Networking and Communication, Anaheim, CA, USA, February 2015. This work was supported by the National Science Foundation under the grants NSF-CCF 1117174 and NSF-ECCS 1102357, and by the European Commission under the grant MC-CIG PCIG12-GA-2012-334213. The associate editor coordinating the review of this paper and approving it for publication was W. Gerstacker.

A. Salim is with the School of Electrical, Computer and Energy Engineering (ECEE), Arizona State University, Tempe, AZ 85287-5706 USA (e-mail: assalim@asu.edu).

T. M. Duman is with the Department of Electrical and Electronics Engineering (EEE), Bilkent University, Ankara, 06800, Turkey, on leave from the School of Electrical, Computer and Energy Engineering (ECEE), Arizona State University, Tempe AZ 85287-5706 USA.

Color versions of one or more of the figures in this paper are available online at http://ieeexplore.ieee.org.

Digital Object Identifier 10.1109/TWC.2015.2413776

over all subcarriers. This is done by computing the optimal relay beamforming vectors and the users' optimal power distribution across all subcarriers. In [7], the authors derive a sliding window estimator to find the optimal timing for taking the discrete Fourier transform (DFT) at the relay to minimize the interference plus noise power. For a UWA-TWR system, three schemes are proposed in [8] to obtain network-coded channel-uncoded packets at the relay. However, a large guard interval that depends on the delay spread and the relative delay between the users' signals is required. An effective OFDM-based solution for asynchronism is proposed in [9] for single-way relay channels with two relays. By relying on full-duplex nodes, this scheme uses a CP that is independent of the relative difference between the propagation delays of the streams at any node.

Previous solutions proposed for asynchronous dual-relay TWR systems have only considered small delays and hence they are not appropriate for the case of large delays, for instance, for typical UWA communications. To the best of our knowledge, the best reported result on this issue is due to [5] which still does not provide a general solution to the large delay problem as it is limited to the case in which the differences in propagation delays are within the CP of an OFDM word. Therefore, motivated by the work in [9] for single-way relay channels, this paper proposes a number of TWR schemes that can be used over a UWA channel or other channels in which large differences in delays may be experienced. The objective is to design an efficient scheme that does not require an excessively long CP and at the same time can tolerate any delay without a large increase in complexity. We aim to avoid the "delay within CP" requirement that is generally assumed in the literature of OFDM-based TWR systems, e.g., [2], [3], [5].

Our approach to address the large delay issue in DTWR systems is to have the received signal on each subcarrier in a delay-diversity structure similar to that observed in single carrier systems over a multipath fading channel in which the signal spreads over time causing symbols to interfere with each other. We will show that with proper signaling, a delay diversity structure is obtained from the frequency domain samples corresponding to the same subcarrier of the consecutively received OFDM words. This structure can be efficiently harnessed at the receiver using the Viterbi algorithm. The original delay diversity scheme, proposed in [10], is based on deliberately introducing multi-path distortion to indirectly obtain a transmit diversity advantage. This is done using a multi-input single-output (MISO) system with M antennas by transmitting the tth symbol from antenna 1 in time slot t and $M-1$ delayed versions of it from antennas 2 through M in time slots $t+1$ to $t+M-1$. In our scheme, the delay diversity structure comes as a by-product of having large differences in delay causing OFDM blocks corresponding to different time slots to interfere with each other.

We consider two cases: full-duplex (FD) operation at all nodes, and full-duplex users with half-duplex (HD) relays. By utilizing the reception period in HD relays to mimic a zero-padded sequence, the second scheme avoids using a CP for the relays' transmission, and as a result, it reduces the complexity of the relays while maintaining the same spectral efficiency compared to the scheme with FD relays, and with only a small degradation in performance.

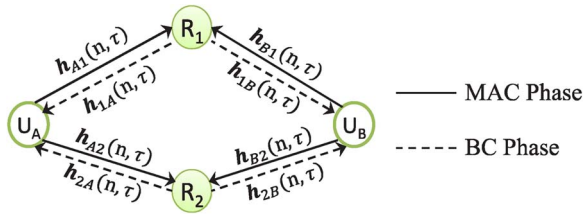

Fig. 1. The DTWR system model.

The remainder of this paper is organized as follows. Section II gives a description of the system model. Section III presents our proposals for harnessing delay diversity using full-duplex and half-duplex relays, respectively. Section IV provides pair-wise error probability (PEP) analysis of the proposed schemes. Section V presents results of simulations conducted to evaluate the performance benefits of the proposed solutions compared to the existing alternatives. Finally, conclusions are drawn in Section VI.

Notation: Unless stated otherwise, bold-capital letters refer to frequency-domain vectors, bold-lower case letters refer to time-domain vectors, capital letters refer to matrices or elements of frequency-domain vectors (depending on the context), and lower-case letters refer to scalars or elements of time-domain vectors. F is the normalized DFT matrix of size-N. The Inverse DFT (IDFT) matrix of size-N is denoted by F^H. The notation $\mathbf{0}_N$ refers to length-N all-zero column vector. The subscript "ir" refers to the channel from node i to node r, $i,r \in \{1,2,A,B\}$, e.g. the subscript "$A2$" refers to the channel from user A to relay 2. The subscript "ArB" refers to the link from node A to node B through node r. The modulo operation that returns the modulus after division of a by b is denoted by $\mathrm{mod}\,(a,b)$. The operator $\mathrm{Bdiag}\{.\}$ returns the block diagonal matrix of the matrices in its argument.

II. System Model and Preliminaries

A. Transmission Model

Two full-duplex users U_A and U_B, which have no direct link between them, exchange their information through two relay nodes R_1 and R_2 (with no link between them), as shown in Fig. 1. Note that the assumption of having two relays is only to simplify the exposition. The obtained results can be easily extended to the multi-relay case. At each user, a standard OFDM modulator with N subcarriers is used. The resulting sequence is appended with a CP of length N_{CP}. Each user transmits M blocks each of length $N+N_{\mathrm{CP}}$ (referred to as a frame), and consecutive frames are separated by sufficient guard times such that no frame affects another.

We consider two-phase amplify-and-forward (AF) relaying which is also referred to as analog network coding (ANC) [11]. In ANC, users exchange data by first simultaneously transmitting their messages to the relay during the multiple-access (MAC) phase. The relay then broadcasts an amplified version of its received signal which is a noise-corrupted summation of the users' messages. This is referred to as the broadcast (BC) phase.

Other relaying strategies are also used in the literature, for instance, [12] uses compute-and forward relaying which maps the superimposed signal at each relay to some noise-free symbol, e.g., the modulo-2 sum of the users' binary bits. However, here we adopt ANC to simplify the operations at the relay nodes.

The time-varying multipath fading channels are modeled by the discrete channel impulse responses (CIRs) $h^n_{ir,l}$ from node i to node r, $n \in \mathbb{Z}^+$, $l \in \{1, 2, \ldots, L_{ir}\}$ where $L_{ir}, i, r \in \{A, B, 1, 2\}$, $i \neq r$, represents the maximum delay spread (length) of the impulse response of the specified channel normalized by the sampling period T_S. We assume that the taps are sample-spaced. The CIRs $h^n_{ir,l}$ represent the response of the respective channels at time n to an impulse applied at time $n - l$. The overall channel response affecting the nth input sample over the L_{ir} lags can be expressed as:

$$\boldsymbol{h}_{ir}(n, \tau) = \sum_{l=1}^{L_{ir}} h^n_{ir,l} \delta(\tau - \tau_{ir,l}), \tag{1}$$

where $\delta(.)$ is the Dirac delta function, τ is the lag index and $\tau_{ir,l}$ is the delay of the lth path normalized by the sampling period T_S. Our model assumes that $\{h^n_{ir,l}\}_{l \in \{1,2,\ldots,L_{ir}\}}$ are circularly symmetric complex Gaussian wide sense stationary processes with zero mean and total envelope power of $\sigma^2_{ir,l}$ which are correlated over time but independent for different lags. Furthermore, all the channels are independent from each other and the CIRs are normalized such that $\sum_{l=1}^{L_{ir}} \sigma^2_{ir,l} = 1$. The effect of unequal gain links is reflected by allowing for different transmission powers and amplification factors at the users and the relays, respectively. We denote the transmission power at the ith user, $i \in \{A, B\}$, by P_i and the amplification factor at the rth relay, $r \in \{1, 2\}$, by G_r.

B. Delay Model

In an asynchronous DTWR system operating over a multi-path channel, two types of timing errors may exist [5]. The first one is due to misalignment of the users' signals at one relay in the MAC phase. The second one is because the signals sent by the relays in the BC phase arrive at different times at a user. Fig. 2 shows an example of the first type of timing errors where the two users' misaligned frames are superimposed over each other (they are shown separately to demonstrate the individual delays). Here, D_{ir}, $i \in \{A, B\}$ and $r \in \{1, 2\}$, denote the propagation delays over the corresponding channels (in units of samples), d_r is the residual delay at the rth relay in samples, $d_r = \text{mod}\,(D_{Br} - D_{Ar}, N + N_{\text{CP}})$ and $\boldsymbol{y}_{ir}$, $i \in \{A, B\}$, $r \in \{1, 2\}$, is the portion of the signal received at the rth relay that corresponds to the message of user i after passing through the channel in the MAC phase.

We assume that the users have full knowledge of the channels and the delays they require, for instance, user B requires all the channels except $\boldsymbol{h}_{1A}(n, \tau)$ and $\boldsymbol{h}_{2A}(n, \tau)$ and all the delays except D_{1A} and D_{2A}. Further, while the rth half-duplex relay requires the knowledge of D_{ir}, $i \in \{A, B\}$, full-duplex relays do not require any delay knowledge. The relays do not require channel knowledge. We also assume, without loss of generality, that $D_{Br} > D_{Ar}$, $r \in \{1, 2\}$ and $D_{i2} > D_{i1}$, $i \in \{A, B\}$. We comment on the effect of estimation errors in propagation delays (and also in channel gains) on the performance in Section V.

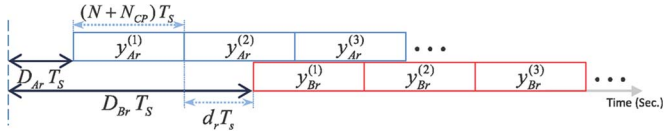

Fig. 2. An example of the signal structure at the rth relay in an asynhchronous DTWR.

III. Proposed Relaying Schemes

In this section, we propose two relaying schemes both based on performing ANC at the relay nodes but with different duplexing methods. The first one uses FD relays, and hence we refer to it as the ANC-FD scheme. In the other one, the receivers of the end-users are designed in a way that allows using HD relays, and hence we call it the ANC-HD scheme.

Transmission from the users is similar in both ANC-FD and ANC-HD schemes (as described in Section II). However, the operations performed by the relays and by the end-users upon reception differ as described in the rest of this section.

A. A DTWR System With Full-Duplex Relays (ANC-FD)

In our first proposal, all the nodes operate in a full duplex mode. After performing IDFT on each frequency-domain data vector, each user appends a CP to the resulting vector and then broadcasts it. Each relay then uses amplify-and-forward on the superimposed signal that is possibly composed of misaligned blocks. At the end of the broadcast phase, each user receives the summation of the signals transmitted by the two relays. With the knowledge of the channel gains and delays, each user removes its self interference which consists of two faded copies of its own signal. After that, each user performs DFT and then uses a Viterbi algorithm to effectively extract delay diversity out of the two copies of its partner's signal. We note that this proposal is an extension of the one in [9] which considers single-way relaying only. This extension necessitates mitigating the relative difference of propagation delays at the relays by properly selecting the CP length and also removing the self-interference components at the end-users.

A full description of the operation of the ANC-FD scheme is given in a recent conference paper [13].

B. A DTWR System With Half-Duplex Relays (ANC-HD)

By performing simple operations at the relays and the end-users, the ANC-HD scheme can use HD relays while providing the same temporal efficiency provided by ANC-FD and incurring only a small performance degradation as will be demonstrated in the sequel.

Define BD_r as the effective OFDM block delay (in samples) between the blocks received from the two users at the rth relay, $BD_r = \left\lfloor \frac{D_{Br} - D_{Ar}}{N + N_{\text{CP}}} \right\rfloor + \left\lfloor \frac{d_r}{N_{\text{CP}} - L_{\text{MAC}}} \right\rfloor$, where $d_r = \text{mod}\,(D_{Br} - D_{Ar}, N + N_{\text{CP}})$ and $L_{\text{MAC}} = \max_{i,r}\{L_{ir} - 1\}$,

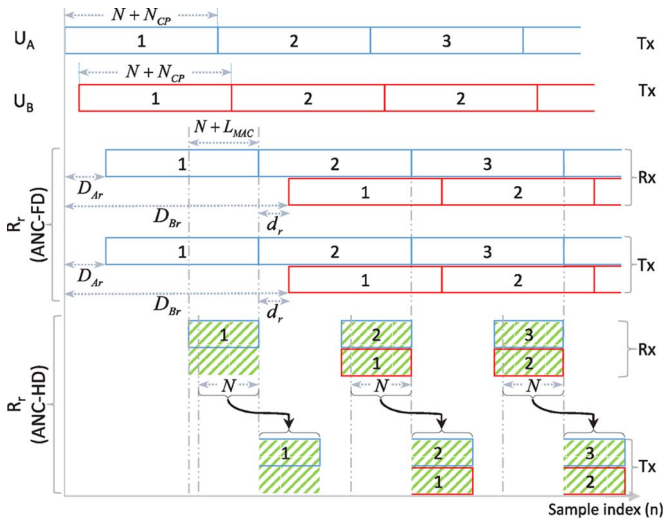

Fig. 3. Timing diagram of the relay operations for both ANC-FD and ANC-HD (with $d_r < N + L_{\mathrm{MAC}}$).

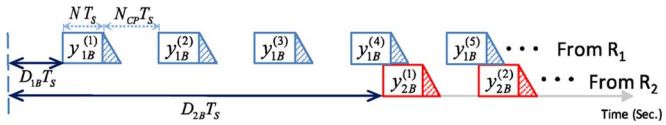

Fig. 4. An example of the structure of the received signal at user B with using ANC-HD.

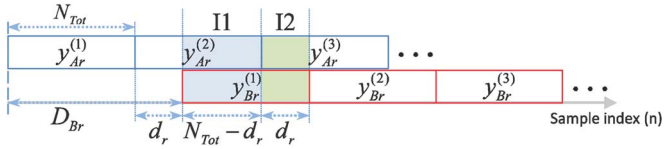

Fig. 5. An example of the signal structure at the rth relay showing the superposition of different parts of blocks originating from users A and B.

$i \in \{A, B\}$ and $r \in \{1, 2\}$. For instance, in Fig. 2, if $d_r > N_{\mathrm{CP}} - L_{\mathrm{MAC}}$, then $BD_r = 2$.

Fig. 3 shows the timing diagram for the relay operations for the ANC-HD scheme where the acronym Tx refers to a transmitted stream while Rx refers to a received one. The figure also shows how the relay forwards the complete set of samples in the case of the ANC-FD scheme. As shown in Fig. 3, in the case of the ANC-HD, each relay selects sequences of length-$(N + N_{\mathrm{CP}})$ seconds starting from the first block in the frame of user A. Depending on the value of d_r, the rth relay, R_r, obtains the appropriate window by choosing specific $(N + L_{\mathrm{MAC}})$ samples from each of the length-$(N+N_{\mathrm{CP}})$ sequences. If $d_r < N+L_{\mathrm{MAC}}$, R_r chooses the last $(N + L_{\mathrm{MAC}})$ samples of each interval; otherwise, it chooses the first $(N + L_{\mathrm{MAC}})$ samples. In both cases, R_r, then removes the first L_{MAC} of the obtained $(N+L_{\mathrm{MAC}})$ samples to ensure robustness against inter-block interference (IBI) and simply amplifies and broadcasts the remaining N samples without appending a cyclic-prefix. After that, each relay remains silent for $(N_{\mathrm{CP}} - N - L_{\mathrm{MAC}})T_s$ seconds. Note that in the ANC-FD scheme, the received signal at the end-user has a CP which simplifies the selection of the DFT window. However, the relays in ANC-HD do not append a CP which makes the received signals at the end-user resemble zero-padded OFDM transmission, which in turn, necessitates performing a cut-and-accumulate (CA) procedure to have the proper DFT window as will be described. Without loss of generality, we consider the case of $d_r < N + L_{\mathrm{MAC}}$ to detail the proposed scheme further. The case of $d_r \geq N + L_{\mathrm{MAC}}$ is only different in terms of the resulting amount of circular shift in time domain or, equivalently, the phase shift in frequency domain.

As seen in Fig. 3, the half-duplex operation of the relays in the ANC-HD scheme is possible because we split the time corresponding to the transmission period of one OFDM block along with its CP from the users into two parts, and with proper timing, less than half of that time is required to have an overlapping window between the blocks coming from the two users in the MAC phase. Using the proposed transmission scheme that avoids a CP for the relays, each relay can broadcast its signal in the remaining time. However, we still require the users to be full-duplex due to two reasons. Firstly, for the relay to guarantee having the minimum overlap window (if there are overlapping blocks), the users should be transmitting their signals continuously without stopping for reception. Secondly, since arbitrary delays can take place and also since no CP is used at the relays, the end-user needs to be able to continuously listen to the channel to receive all the signals transmitted by the relays.

The structure of the received signal at user B, for example, will be of the form shown in Fig. 4 where D_{rB}, $r \in \{1, 2\}$, is the propagation delay experienced over the link from the rth relay to user B. Shaded parts of the blocks in Fig. 4 represent the tailing sequence which is the portion of the received block due to multipath fading after the signal has been linearly convolved with the channel impulse response. We can see that what user B observes from each relay is a silence period along with an active period that consists of the N data samples and the tailing sequence. Without loss of generality, we assume that $D_{2B} > D_{1B}$. With the knowledge of D_{Br}, D_{rB}, $\boldsymbol{h}_{Br}(n, \tau)$ and $\boldsymbol{h}_{rB}(n, \tau)$, $r \in \{1, 2\}$, user B can subtract its own message, which results in a superimposed signal of its partner's blocks and their delayed version affected by a different channel.

1) Minimum CP Length: In the first phase of the proposed scheme, each relay receives a sum of the signals from the two users with a possible delay between them. In a conventional point to point OFDM system, the transmitter appends a cyclic-prefix of length N_{CP} that is at least equal to the maximum delay spread of the channel such that when the receiver removes the first N_{CP} samples, the IBI is completely removed. Therefore, when there are two signals superimposed over each other, there should be sufficient overlap between the blocks that contains a complete set of the users' samples plus a number of samples sufficient enough to ensure that no residual samples from previous blocks (i.e. IBI) are affecting the current block.

Let N_{Tot} denote the total number of samples in a block including the CP, i.e., $N_{Tot} = N + N_{\mathrm{CP}}$. Referring to Fig. 5 wherein we assume $D_{A1} = 0$, the intervals I1 and I2 show the superposition of different parts of blocks originating

from users A and B. To guarantee having the proper window for any value of d_r, there should be at least an $N + L_{\rm MAC}$ sample overlap window in either I1, I2 or both. In other words, we should have $N_{Tot} - d_r \geq N + L_{\rm MAC}$ or $d_r \geq N + L_{\rm MAC}$. To accommodate any value of d_r, we remove its effect on selecting the value of N_{Tot} by substituting the second inequality into the first one which gives $N_{Tot} \geq 2N + 2L_{\rm MAC}$. Therefore, choosing a CP length at the users that satisfies $N_{\rm CP} \geq N + 2L_{\rm MAC}$ enables each relay to have at least $N + L_{\rm MAC}$ samples overlap between the two users' misaligned blocks and hence guarantees proper operation at the relay during the MAC phase. Moreover, our system imposes another condition for the second phase, where the length-$N_{\rm CP}$ period following the length N transmission period should be at least equal to L_{BC} where $L_{BC} = \max_{i,r}\{L_{ri} - 1\}$, $r \in \{1, 2\}$ and $i \in \{A, B\}$. Also, as we will note while deriving the cut-and-accumulate procedure, we require $N_{\rm CP}$ to be greater than $N + L_{1B} + L_{2B} - 2$. Therefore, to simultaneously combat the frequency selectivity and the timing errors for the ANC-HD scheme, each user precedes each of its blocks by a CP of length $N_{\rm CP}$ that satisfies

$$N_{\rm CP} \geq \max\{\max_{i,r} N + 2L_{ir} - 2,\ \max_{i,r} L_{ri} - 1, \\ N + L_{1B} + L_{2B} - 2\}, \quad (2)$$

where $i \in \{A, B\}$ and $r \in \{1, 2\}$. Note that the $N_{\rm CP}$ criterion does not depend on the relative propagation delay even if it spans over multiple OFDM blocks; it only depends on the number of subcarriers and length of the channels. This actually explains why our ANC-HD scheme outperforms the systems in [5] and [2] as will be detailed in Section V.

2) Relay Processing: Assuming a discrete baseband model, the data vector representing the frequency-domain message of the ith user, $i \in \{A, B\}$, during the mth block is denoted by $\boldsymbol{X}_i^{(m)} = [X_{i,1}^{(m)}, X_{i,2}^{(m)}, \ldots, X_{i,N}^{(m)}]^T$ where $X_{i,k}^{(m)} \in \mathcal{A}_i$ for $k \in \{1, 2, \ldots, N\}$ and $\mathcal{A}_i$ is the signal constellation for user i. Taking the IDFT, we obtain $\boldsymbol{x}_i^{(m)} = \text{IDFT}(\boldsymbol{X}_i^{(m)})$ where $\boldsymbol{x}_i^{(m)} = [x_{i,1}^{(m)}, x_{i,2}^{(m)}, \ldots, x_{i,N}^{(m)}]^T$, $i \in \{A, B\}$. The transmitted signal from the ith user during the mth block, $i \in \{A, B\}$, is given by $\boldsymbol{x}_{T,i}^{(m)} = \sqrt{P_i}\zeta(\boldsymbol{x}_i^{(m)})$ where $\boldsymbol{x}_{T,i}^{(m)} = [x_{T,i,1}^{(m)}, x_{T,i,2}^{(m)}, \ldots, x_{T,i,N+N_{\rm CP}}^{(m)}]^T$ and $\zeta(\cdot)$ corresponds to the operation of appending a length-$N_{\rm CP}$ cyclic-prefix to the vector in its argument.

For the rth relay, the received signal at the nth sample, $n \in \{1, 2, \ldots, N\}$, during the m_r^{th} window, $m_r \in \{1, 2, \ldots, M + BD_r\}$, is given by

$$y_{r,n}^{(m_r)} = \sqrt{P_A}\sum_{l=1}^{L_{Ar}} x_{T,A,n+N_{\rm CP}-l+1}^{(m_r)} h_{Ar,l}^{(m_r-1)N+m_rN_{\rm CP}+n-l+D_{Ar}+1} + \sqrt{P_B}\sum_{l=1}^{L_{Br}} x_{T,B,n+N_{\rm CP}-l-d_r+1}^{(m_r-BD_r)} h_{Br,l}^{(m_r-1)N+m_rN_{\rm CP}+n-l+D_{Br}+1} + n_{r,n}^{(m_r)} \quad (3)$$

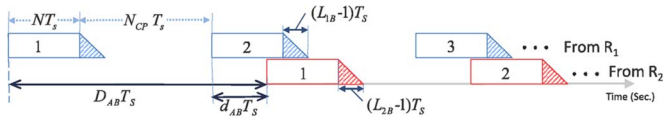

Fig. 6. An example of the structure of $\boldsymbol{y}_{AB,e}$ with one block delay.

where $n_{r,n}^{(m_r)}$ is the noise at the rth relay during the m_r^{th} block modeled by a complex circularly symmetric Gaussian random variable with zero mean and variance σ_r^2. Note that $x_{T,i,n}^m = 0$ if $n < 1$, $n > N + N_{\rm CP}$, $m < 1$ or $m > M$. We can write (3) in vector form as

$$\boldsymbol{y}_r^{(m_r)} = \sqrt{P_A}H_{tl,Ar}^{(m_r)}\boldsymbol{x}_A^{(m_r)} + \sqrt{P_B}\Psi_{d_r}H_{tl,Br}^{(m_r-BD_r)}\boldsymbol{x}_B^{(m_r-BD_r)} + \boldsymbol{n}_r^{(m_r)},$$

where $\boldsymbol{y}_r^{(m_r)} = [y_{r,1}^{(m_r)}, y_{r,2}^{(m_r)}, \ldots, y_{r,N}^{(m_r)}]^T$, Ψ_{d_r} is a circulant matrix of size $N \times N$ whose first column is given by the $N \times 1$ vector $\psi_{d_r} = [\boldsymbol{0}_{d_r}^T, 1, \boldsymbol{0}_{N-d_r-1}^T]^T$ and $\boldsymbol{n}_r^{(m_r)} = [n_{r,1}^{(m_r)}, n_{r,2}^{(m_r)}, \ldots, n_{r,N}^{(m_r)}]^T$. Using the matrix Ψ_{d_r} is equivalent to performing circular convolution with ψ_{d_r}, which on the other hand mimics the circular shift caused by selecting the window in a location that has the samples of the blocks of user B circularly shifted from their original order. Note that $\boldsymbol{x}_B^{(m_r-BD_r)} = \boldsymbol{0}_N$ for $m_r \leq BD_r$.

The matrix $H_{tl,ir}^{(m_r)}$, $i \in \{A, B\}$, $r \in \{1, 2\}$ and $m_r \in \{1, 2, \ldots, M + BD_r\}$ is the time-lag channel matrix which is also known as the time-variant circular convolution matrix. This matrix represents the time-domain effect of circular convolution of $\boldsymbol{x}_i^{(m_r)}$ with $\boldsymbol{h}_{ir}(n, \tau)$ for all the N samples in the selected window during the $m_r{}^{th}$ block after discarding the first $L_{\rm MAC}$ samples. By looking at the received signal at the rth relay when $L_{ir} < N$, we note that $H_{tl,ir}^{(m_r)}$ has the structure given in (5), shown at the bottom of the next page, where $N_r = N_{\rm CP} + (m_r - 1)N_{Tot}$.

Note that (5) has been derived for the case that $L_{ir} < N$. However, the structure of $H_{tl,ir}^{(m_r)}$ when $L_{ir} \geq N$ can be similarly obtained. In case of quasi-static channels or for block fading channels where the channel remains fixed for each OFDM block but changes from one block to another, $H_{tl,ir}^{(m_r)}$ is equal to the conventional time-invariant circular convolution matrix.

Upon receiving $\boldsymbol{y}_r^{(m_r)}$, the transmitted signal by the rth relay is given by $\boldsymbol{x}_r^{(m_r)} = \sqrt{G_r}\boldsymbol{y}_r^{(m_r)}$, $r \in \{1, 2\}$. Note that the relay does not append a CP, it simply amplifies and forwards the selected windows from its received signal.

3) Receiver Design: This section discusses the operations performed at each user while receiving the sum of the relays' signals where the objective of each user is to detect its partner's message. We consider the processing at user B. Similar arguments can be stated for user A due to symmetry.

Fig. 6 shows an example of the received signal structure at user B after the self-interference is removed, i.e., $\boldsymbol{y}_{AB,e}$ which represents the effective message of user A at user B after passing through the channel. Note that this signal is composed of two parts each relayed by one of the relays. As shown in

Fig. 6, at user B, the frame relayed by R_2 is received $D_{\rm AB}$ sample times after the frame relayed by R_1 where $D_{\rm AB} = (D_{A2} + D_{2B}) - (D_{A1} + D_{1B})$. The effective signal from user A for the whole frame can be expressed as

$$\boldsymbol{y}_{AB,e} = \left[\boldsymbol{y}_{A1B,e}^T, \mathbf{0}_{D_{\rm AB}}^T\right]^T + \left[\mathbf{0}_{D_{\rm AB}}^T, \boldsymbol{y}_{A2B,e}^T\right]^T + \boldsymbol{w}_B \quad (4)$$

where $\boldsymbol{y}_{ArB,e}$, $r \in \{1,2\}$, is the portion of $\boldsymbol{y}_{AB,e}$ that corresponds to the message of user A after passing through the channel and getting relayed by the rth relay. The vector $\boldsymbol{w}_B$ represents length-$(N+N_{\rm CP})(M+BD_{\rm AB})$ noise vector at user B which encompasses the relays' amplified noise as well. Its entries are assumed to be independent and identically distributed (i.i.d.) complex circularly symmetric Gaussian random variables with zero mean and variance σ_B^2. Let $d_{\rm AB}$ denote the residual delay in samples as shown in Fig. 6 where $d_{\rm AB} = \mod(D_{\rm AB}, N+N_{\rm CP})$. Depending on the value of $d_{\rm AB}$, different parts of the users' blocks overlap and hence each value of $d_{\rm AB}$ should be treated accordingly. We identify the following ranges for $d_{\rm AB}$:

- case 1: $0 \le d_{\rm AB} < N + (L_{1B} - 1)$,
- case 2: $N + (L_{1B} - 1) \le d_{\rm AB} \le N_{\rm CP} - (L_{2B} - 1)$,
- case 3: $N_{\rm CP} - (L_{2B} - 1) < d_{\rm AB} < N + N_{\rm CP}$.

We note that case 1 and case 3 take place when there is an overlap between the blocks of user A with those of user B. In case 1, the blocks of user A lead those of user B, while they lag behind them in case 3. On the other hand, Case 2 represents the situation of having no overlap.

We define $BD_{\rm AB} = \left\lfloor \frac{D_{\rm AB}}{N+N_{\rm CP}} \right\rfloor + \left\lfloor \frac{d_{\rm AB}}{N_{\rm CP}-(L_{2B}-1)} \right\rfloor$ as the effective OFDM block delay observed at user B between the blocks received from the two relays that correspond to the message of user A. For the first and last $BD_{\rm AB}$ blocks there are blocks from one of the relays only and hence conventional techniques developed for zero-padded OFDM can be used to mimic circular convolution [14]. However, for the remaining blocks, since the relays do not append a CP, we propose a cut-and-accumulate procedure to mimic the effect of the CP in converting the linear convolution with the CIR into a circular

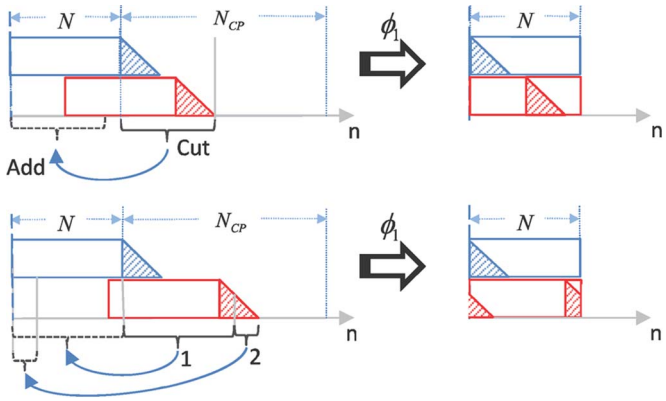

Fig. 7. The CA procedure for case 1 with various values of $d_{\rm AB}$.

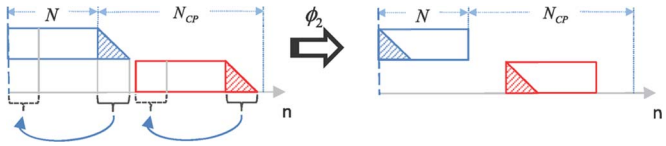

Fig. 8. The CA procedure for case 2.

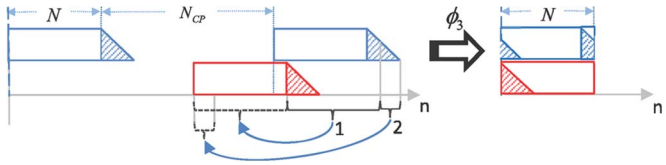

Fig. 9. An example of the CA procedure for case 3.

one. Figs. 7–9 illustrate how to perform the CA procedure for the different cases of $d_{\rm AB}$ wherein the operator $\phi_c(\cdot)$, $c \in \{1,2,3\}$ denotes the modulo-N vector accumulator used for the cth case. Note that the two frames are superimposed over each other, however, we show them separated to simplify our exposition. For case 1, $\phi_1(\cdot)$ takes a length $l_a = N + \max\{L_{1B} - 1, d_{\rm AB} + L_{2B} - 1\}$ vector, then selects and accumulates the first $N_N = \left\lfloor 1 + \frac{d_{\rm AB}+L_{2B}-1}{N} \right\rfloor$ sequences of

$$H_{ll,ir}^{(m_r)} = \begin{bmatrix}
h_{ir,1}^{1+N_r} & 0 & \cdots & \cdots & \cdots & 0 & h_{ir,L_{ir}}^{N_r-L_{ir}+2} & \cdots & \cdots & h_{ir,3}^{N_r-1} & h_{ir,2}^{N_r} \\
h_{ir,2}^{1+N_r} & h_{ir,1}^{2+N_r} & 0 & \cdots & \cdots & \cdots & 0 & h_{ir,L_{ir}}^{N_r-L_{ir}+3} & \cdots & \cdots & h_{ir,3}^{N_r} \\
\vdots & h_{ir,2}^{2+N_r} & \ddots & \ddots & & & \ddots & \ddots & \ddots & & \vdots \\
h_{ir,L_{ir}}^{1+N_r} & \vdots & \ddots & \ddots & \ddots & & & \ddots & \ddots & & h_{ir,L_{ir}}^{N_r} \\
0 & h_{ir,L_{ir}}^{2+N_r} & \ddots & \ddots & \ddots & \ddots & & & \ddots & & 0 \\
\vdots & 0 & \ddots & \ddots & \ddots & \ddots & \ddots & & & 0 & \vdots \\
\vdots & \vdots & & \ddots & \ddots & \ddots & \ddots & \ddots & & h_{ir,1}^{N+N_r-1} & 0 \\
0 & 0 & \cdots & \cdots & 0 & h_{ir,L_{ir}}^{N+N_r-L_{ir}+1} & \cdots & \cdots & \cdots & h_{ir,2}^{N+N_r-1} & h_{ir,1}^{N+N_r}
\end{bmatrix} \quad (5)$$

length-N on a sample-by-sample basis with a length-N zero-padded sequence containing the last $l_a - N_N N$ samples. N_N is simply the number of length-N vectors in the length-l_a interval. For instance, in the first example of Fig. 7, $l_a = N + d_{\rm AB} + L_{2B} - 1$ and $N_N = 1$. Note that in case 1, the accumulator is aligned with the blocks relayed by R_1. Mathematically, this accumulator can be expressed by

$$\begin{aligned}&\phi_1(\boldsymbol{x})\\&=\sum_{i=1}^{N_N}\left[\boldsymbol{x}\left(1+(i-1)N\right),\ \boldsymbol{x}\left(2+(i-1)N\right),\ldots,\boldsymbol{x}(iN)\right]^T\\&\quad+\left[\left[\boldsymbol{x}(1+N_N N),\boldsymbol{x}\left(2+N_N N\right),\ldots,\boldsymbol{x}(l_a)\right],\mathbf{0}^T_{(N_N+1)N-l_a}\right]^T,\end{aligned}$$

where $\boldsymbol{x}$ and $\phi_1(\boldsymbol{x})$ are length-l_a and length-N column vectors, respectively. Fig. 7 shows the effect of applying the CA procedure for various values for the residual delay $d_{\rm AB}$.

For case 3, the current block from the frame relayed by R_2 starts overlapping with the next block from the frame relayed by R_1, hence the accumulator $\phi_3(\cdot)$ operates on its input similar to $\phi_1(\cdot)$ with the difference that the accumulator is aligned with the blocks relayed by R_2 rather than R_1. Note that if $N_{\rm CP}$ is less than $N + L_{1B} + L_{2B} - 2$, then, for $d_{\rm AB}$ values falling within case 3 there will be IBI, and hence we impose the condition $N_{\rm CP} \geq N + L_{1B} + L_{2B} - 2$ in (2).

After $\boldsymbol{y}_{AB,e}$ is passed through the cut-and-accumulate block, the resulting N-sample OFDM blocks, $\{\boldsymbol{y}^{(m)}_{\rm AB}\}$, $m \in \{1,2,\ldots,M+BD_{AB}\}$, can be written as

$$\begin{aligned}\boldsymbol{y}^{(m)}_{\rm AB} &= \sqrt{P_{A1}}H^{(m)}_{tl,A1B}\boldsymbol{x}^{(m)}_A\\&\quad+\sqrt{P_{A2}}\Psi_{d_{\rm AB}}H^{(m-BD_{\rm AB})}_{tl,A2B}\boldsymbol{x}^{(m-BD_{\rm AB})}_A+\boldsymbol{v}^{(m)}_B,\end{aligned}\quad(6)$$

where $P_{Ar} = P_A G_r$, $\boldsymbol{x}^{(m)}_A = \mathbf{0}_N$ for $m < 1$ and $m > M$, $H^{(m)}_{tl,ArB} = H^{(m)}_{tl,rB}H^{(m)}_{tl,Ar}$, $r \in \{1,2\}$, is the equivalent time-lag channel matrix corresponding to the link from user A through the rth relay to user B. Note that the matrices $H^{(m)}_{tl,rB}$, $r \in \{1,2\}$, that correspond to the BC phase have the same structure of the matrices $H^{(m)}_{tl,Ar}$, $r \in \{1,2\}$, which correspond to the MAC phase. However, the matrices $H^{(m)}_{tl,rB}$ $r \in \{1,2\}$ are formed assuming a cyclic-suffix rather than a cyclic-prefix due to the CA procedure. The vector $\boldsymbol{v}^{(m)}_B$ represents length-N effective noise vector at user B during the mth block after performing the CA procedure. The entries of $\boldsymbol{w}_B$ in (4) are i.i.d. whereas the entries of $\boldsymbol{v}^{(m)}_B$ in (6) are no longer identically distributed, but they are independent. The reason is that while performing the CA procedure, the noise samples get accumulated different number of times. The first $l_a - N_N N$ noise samples of each block get accumulated with the $l_a - N_N N$ noise samples that were cut, which means that the first $l_a - N_N N$ noise samples are complex Gaussian random variables with zero mean and variance of $(N_N+1)\sigma^2_B$, while the other samples of the final length-N block have a variance of $N_N\sigma^2_B$.

Looking at case 1, for instance, it is clear that the samples of the blocks relayed by R_2 have been circularly shifted by $d_{\rm AB}$ samples. Since having a delay of n samples in the time domain causes the kth subcarrier to have a phase shift of $e^{-j2\pi n(k-1)/N}$, $k \in \{1,2,\ldots,N\}$, we can define the frequency-domain phase shift vector corresponding to a $d_{\rm AB}$-sample delay in time as $\boldsymbol{g}_{d_{\rm AB}} = \left[1, e^{-j\frac{2\pi d_{\rm AB}}{N}},\ldots,e^{-j\frac{2\pi d_{\rm AB}(N-1)}{N}}\right]^T$. Each block of the accumulated signal is then demodulated by an N-point DFT module. After DFT, the mth block can be written in frequency-domain as

$$\begin{aligned}\boldsymbol{Y}^{(m)}_{\rm AB} &= \sqrt{P_{A1}}FH^{(m)}_{tl,A1B}F^H\boldsymbol{X}^{(m)}_A\\&\quad+\sqrt{P_{A2}}F\Psi_{d_{\rm AB}}H^{(m-BD_{\rm AB})}_{tl,A2B}F^H\boldsymbol{X}^{(m-BD_{\rm AB})}_A+F\boldsymbol{v}^{(m)}_B\\&=\sqrt{P_{A1}}H^{(m)}_{sc,A1B}\boldsymbol{X}^{(m)}_A\\&\quad+\sqrt{P_{A2}}\left(H^{(m-BD_{\rm AB})}_{sc,A2B}\boldsymbol{X}^{(m-BD_{\rm AB})}_A\right)\circ\boldsymbol{g}_{d_{\rm AB}}+\boldsymbol{V}^{(m)}_B,\end{aligned}\quad(7)$$

where F is the normalized DFT matrix of size-N, the operator $\circ$ denotes the Hadamard product, $[Z\circ W]_{i,j} = [Z]_{i,j}\cdot[W]_{i,j}$, and $\boldsymbol{V}^{(m)}_B = [V^{(m)}_{B,1}, V^{(m)}_{B,2},\ldots,V^{(m)}_{B,N}]^T = F\boldsymbol{v}^{(m)}_B$. The elements of $\boldsymbol{V}^{(m)}_B$ are correlated zero-mean complex Gaussian random variables. The covariance matrix of $\boldsymbol{V}^{(m)}_B$ is given by $F\Sigma F^H$ where $\Sigma = \text{diag}\{[(N_N+1)\sigma^2_B, (N_N+1)\sigma^2_B,\ldots,(N_N+1)\sigma^2_B]_{1\times(l_a-N_N N)}, [N_N\sigma^2_B, N_N\sigma^2_B,\ldots,N_N\sigma^2_B]_{1\times((N_N+1)N-l_a)}]\}$. The matrix $H^{(m)}_{sc,ArB}$ is the subcarrier coupling matrix for the mth block over the U_A-R_r-U_B link [15]. This matrix gives a glimpse of the effect of the channel in frequency-domain and it is found using the time-lag matrices of the corresponding channels or their frequency-domain counterparts as:

$$\begin{aligned}H^{(m)}_{sc,ArB} &= FH^{(m)}_{tl,ArB}F^H = FH^{(m)}_{tl,rB}H^{(m)}_{tl,Ar}F^H\\&= FH^{(m)}_{tl,rB}F^HFH^{(m)}_{tl,Ar}F^H = H^{(m)}_{sc,rB}H^{(m)}_{sc,Ar}.\end{aligned}\quad(8)$$

In case of block, and of course quasi-static, fading, $H_{tl,ArB}$, $r \in \{1,2\}$, have a circulant structure making $H_{sc,ArB}$, $r \in \{1,2\}$, diagonal which means that no inter-carrier interference (ICI) is present. When the channel is time-varying within the same OFDM block, neither $H_{tl,ArB}$, $r \in \{1,2\}$, will be circulant nor will $H_{sc,ArB}$, $r \in \{1,2\}$, be diagonal, which means that the subcarrier orthogonality is lost, giving rise to ICI. Here, we do not investigate ICI mitigation, instead we ignore the effects of the off-diagonal elements of $H^{(m)}_{sc,ArB}$ in detection.

Let $q^{(m)}_{r,k} = \sqrt{P_{Ar}}[H^{(m)}_{sc,ArB}]_{k,k}$, $r \in \{1,2\}$. By discarding the off-diagonal elements of $H^{(m)}_{sc,ArB}$, the received signal on the kth subcarrier during the mth block can be written as

$$\begin{aligned}Y^{(m)}_{AB,k} \approx q^{(m)}_{1,k}X^{(m)}_{A,k} &+ e^{-j\frac{2\pi(k-1)d_{\rm AB}}{N}}q^{(m-BD_{\rm AB})}_{2,k}\\&\times X^{(m-BD_{\rm AB})}_{A,k}+V^{(m)}_{B,k},\end{aligned}\quad(9)$$

where $V^{(m)}_{B,k}$ is the kth element of $\boldsymbol{V}^{(m)}_B$. We remark that (9) is exact if the channel is time-invariant within each OFDM block. For case 3, similar arguments made to case 1 can be stated but with the difference that the phase shift correction factor in (9)

will be required for the blocks relayed by R_1 rather than those relayed by R_2 and its value will be $e^{-j\frac{2\pi(k-1)(N+N_{\rm CP}-d_{\rm AB})}{N}}$.

For case 2, there is no overlap between the blocks relayed by the two relays, a fact that motivates using maximum ratio combining (MRC) since we now have two independently faded copies of each OFDM block. As shown in Fig. 8, $\phi_2(\cdot)$ operates on the two parts separately. For the part relayed by the rth relay it takes a length $l_a = N + L_{rB} - 1$ vector, then selects and accumulates the first $N_N = \left\lfloor 1 + \frac{L_{rB}-1}{N} \right\rfloor$ sequences of length-N and adds that to a length-N zero-padded sequence containing the last $l_a - N_N N$ samples. As a result, $\phi_2(\cdot)$ returns two blocks of length-N. After taking their DFT, these blocks can be expressed as

$$\begin{aligned}\boldsymbol{Y}_{A1B}^{(m)} &= \left[Y_{A1B,1}^{(m)}, Y_{A1B,2}^{(m)}, \ldots, Y_{A1B,N}^{(m)}\right]^T \\ &= \sqrt{P_{A1}} H_{sc,A1B}^{(m)} \boldsymbol{X}_A^{(m)} + \boldsymbol{V}_{1B}^{(m)} \\ \boldsymbol{Y}_{A2B}^{(m)} &= \left[Y_{A2B,1}^{(m)}, Y_{A2B,2}^{(m)}, \ldots, Y_{A2B,N}^{(m)}\right]^T \\ &= \sqrt{P_{A2}} H_{sc,A2B}^{(m-BD_{\rm AB})} \boldsymbol{X}_A^{(m-BD_{\rm AB})} + \boldsymbol{V}_{2B}^{(m)}, \end{aligned} \quad (10)$$

where $\boldsymbol{Y}_{ArB}^{(m)}$, $r \in \{1,2\}$, corresponds to the part of the message of user A relayed by the rth relay during the mth interval and $\boldsymbol{V}_{rB}^{(m)} = [V_{rB,1}^{(m)}, V_{rB,2}^{(m)}, \ldots, V_{rB,N}^{(m)}]^T = F\boldsymbol{v}_{rB}^{(m)}$ where $\boldsymbol{v}_{rB}^{(m)}$ is the noise vector whose elements are complex Gaussian random variables with zero mean and variance of $(N_N+1)\sigma_B^2$ for the first $l_a - N_N N$ elements and $N_N\sigma_B^2$ for the remaining ones.

4) Detection of the Partner's Message: For cases 1 and 3, the structure of the received signal in (9) on the kth subcarrier from all the blocks is similar to a single-carrier (SC) multipath channel or equivalently to a MISO system utilizing delay diversity. The receiver extracts this diversity using maximum likelihood sequence detection, implemented efficiently through a Viterbi algorithm. For both ANC-FD and ANC-HD schemes, each user implements N parallel Viterbi detectors of $M_c^{BD_{\rm AB}}$ states where M_c is the constellation size. The kth Viterbi detector is fed with the collected received samples of that subcarrier over the $M + BD_{\rm AB}$ blocks, i.e., $\{Y_{AB,k}^{(m)}\}_{m\in\{1,2,\ldots,M+BD_{\rm AB}\}}$, to detect the symbols sent on the kth subcarrier over the M blocks, $\left\{X_{A,k}^{(m)}\right\}_{m\in\{1,2,\ldots,M\}}$. Clearly, the increase in complexity depends on the number of block delays ($BD_{\rm AB}$) rather than the actual relative propagation delay ($d_{\rm AB}$) which is an advantage of the proposed schemes. Specifically, the complexity of the Viterbi detector is affected by: (i) the number of states ($M_c^{BD_{\rm AB}}$) and (ii) the number of stages which is equal to $M + BD_{\rm AB}$.

Unlike cases 1 and 3, detection for case 2 is done on a symbol-by-symbol basis using MRC. Referring to (10), for each subcarrier, the receiver collects the samples corresponding to the same transmitted symbol in the vector $\boldsymbol{r}_k^{(m)} = [Y_{A1B,k}^{(m)}, Y_{A2B,k}^{(m+BD_{\rm AB})}]^T$. By discarding the ICI, we can write

$$\boldsymbol{r}_k^{(m)} \approx \begin{bmatrix} g_{1,k}^{(m)} \\ g_{2,k}^{(m)} \end{bmatrix} X_{A,k}^{(m)} + \begin{bmatrix} V_{1B,k}^{(m)} \\ V_{2B,k}^{(m+BD_{\rm AB})} \end{bmatrix}, \quad (11)$$

where $g_{r,k}^{(m)} = \sqrt{P_{Ar}}[H_{sc,ArB}^{(m)}]_{k,k}$. Based on MRC, we write the following detection rule to recover $X_{A,k}^{(m)}$

$$\begin{aligned}\hat{X}_{A,k}^{(m)} &= \arg\min_{X\in\mathcal{A}_A} \left| \boldsymbol{r}_k^{(m)} - \begin{bmatrix} g_{1,k}^{(m)} \\ g_{2,k}^{(m)} \end{bmatrix} X \right|^2 \\ &= \arg\max_{X\in\mathcal{A}_A} \left\{ \mathrm{Re}\left\{ {Y_{A1B,k}^{(m)}}^* g_{1,k}^{(m)} X \right\} \right. \\ &\qquad \left. + \mathrm{Re}\left\{ {Y_{A2B,k}^{(m+BD_{\rm AB})}}^* g_{2,k}^{(m)} X \right\} \right\}, \end{aligned} \quad (12)$$

where we have assumed the use of an M-ary phase-shift keying (PSK) constellation in the last step.

C. Maximum Achievable Data Rate

To clearly see the benefit of having a delay-independent CP, we investigate the temporal efficiency of the proposed schemes. Let η denote the maximum achievable data rate when binary PSK (BPSK) modulation is used. The transmission of one OFDM block with either ANC-FD or ANC-HD relaying requires $N + N_{\rm CP}$ samples. Hence, their rate is given by

$$\eta_{\text{ANC-HD}} = \frac{M}{M + BD_{\rm AB}} \cdot \frac{N}{N + N_{\rm CP}}, \quad (13)$$

which shows that the only effect of the delay on $\eta_{\text{ANC-HD}}$ is through the number of block delays $BD_{\rm AB}$ rather than the actual delay $D_{\rm AB}$; an effect that is negligible if M is sufficiently large. To see this advantage, we compare it to some of the existing schemes that solve the asynchrony issue. Specifically, we consider the ANC-STBC scheme in [5] and the ANC-OFDM scheme which is an extension of the system in [2] to the dual-relay case. Noting that the rate for both ANC-STBC and ANC-OFDM is given by $\frac{N}{2N+N_{\rm CP,MAC}+N_{\rm CP,BC}}$, where $N_{\rm CP,MAC}$ and $N_{\rm CP,BC}$ are the minimum CP lengths required for the MAC and BC phases, respectively, we can see that the rate decreases if $D_{\rm AB}$ increases since a longer CP will be needed.

D. Subcarrier Diversity for Small Delays

Both ANC-FD and ANC-HD relaying schemes proposed provide a delay diversity structure that can result in a diversity gain of N_R, where N_R is the number of relays used. However, this gain requires having at least one block delay. To provide a diversity gain for smaller delays wherein $BD_{\rm AB} = 0$ while preserving the same diversity gain for large delays, we propose a modification to the original system as follows: the rth relay does not only amplify and forward its received signal, instead, it also multiplies the nth sample, $n \in \{1, \ldots, N\}$, of the selected window by $e^{j\frac{2\pi(n-1)(r-1)}{N}}$, which will have the effect of having a circular shift of $r-1$ samples in frequency domain due to the modulation property of DFT. By doing so, we will have a subcarrier diversity structure that can be efficiently harnessed using the Viterbi algorithm. This approach will enable our system to attain a diversity order equal to the number of relays (N_R) as long as $N_R \leq N$.

To simplify exposition, we only consider small delays for case 1. Extending the results to the two other cases is straightforward. If we discard the off-diagonal elements of $H^{(m)}_{sc,ArB}$ and assume that $N_R \leq N$, $Y^{(m)}_{AB,k}$ can be written as

$$Y^{(m)}_{AB,k} = q^{(m)}_{1,k} X^{(m)}_{A,k} + \sum_{r=2}^{N_R} e^{-j\frac{2\pi(k-1)D_{\mathrm{AB}}}{N}} q^{(m-BD_{\mathrm{AB}})}_{r,k} X^{(m-BD_{\mathrm{AB}})}_{A,\langle k-r+1\rangle_N} + V^{(m)}_{B,k}, \quad (14)$$

where $q^{(m)}_{r,k} = \sqrt{P_{Ar}}[H^{(m)}_{sc,ArB}]_{k,k}$ and $\langle l\rangle_N$ is the cyclic shift operator defined as

$$\langle l\rangle_N = \begin{cases} N+l, & l \leq 0 \\ l, & l > 0 \end{cases}$$

The subcarrier coupling matrix, $H^{(m)}_{sc,ArB}$, is now defined as $H^{(m)}_{sc,ArB} = H'^{(m)}_{sc,rB} H^{(m)}_{sc,Ar}$ and $H'^{(m)}_{sc,rB} = \theta_r(H^{(m)}_{sc,rB})$ where $\theta_r(\cdot)$ circularly shifts the rows of its argument by $(r-1)$ rows downward. Clearly, unlike the large delay case, we observe a delay structure among the symbols on different subcarriers of the same block as in (14). Hence, the detection is performed on a block-by-block basis, and for each of the M blocks, the receiver drops the first $(N_R - 1)$ symbols and uses a Viterbi detector with $M_c^{N_R-1}$ states. The spectral efficiency loss due to the partial symbol drop is negligible since $N_R \ll N$ in practice.

IV. Pairwise Error Probability Analysis

Motivated by the fact that studying the pairwise error probability can give an insight into the diversity order and also provide a basis for code design, we present in this section some upper bounds on the PEP for the proposed full- and half-duplex relaying schemes. For the half-duplex scheme we restrict our analysis to case 1 and case 3 since case 2 resembles a two-branch single-input multiple-output (SIMO) system whose performance is well-studied in the literature. We consider three cases for the multipath fading channel: quasi-static fading, correlated block fading and independent block fading. We use BPSK modulation and assume that the MAC phase links experience much higher SNRs than those during the BC phase which allows us to discard the effect of the noise terms at the relay nodes. Without loss of generality, we consider detection at user B and assume that $L_{Ar} < N$ and $L_{rB} < N$, $r \in \{1,2\}$. Let $L = \max\{\max_{r\in\{1,2\}} L_{Ar}, \max_{r\in\{1,2\}} L_{rB}\}$.

A. Quasi-Static Frequency-Selective Fading Channels

Given that the self-interference is perfectly eliminated at each user, the proposed ANC-FD scheme resembles the system in [9] that assumes a single-way relay system with two relays. As a result, the PEP results obtained in [9] are applicable. Let us define $\boldsymbol{X}_{A,(k)} = [X^{(1)}_{A,k}, X^{(2)}_{A,k}, \ldots, X^{(M)}_{A,k}]$. Without loss of generality we assume $P_A = 1$. Let $PEP_{A,k} = P(\boldsymbol{X}_{A,(k)} \rightarrow \boldsymbol{X}'_{A,(k)})$ denote the pairwise error probability of two streams $\boldsymbol{X}_{A,(k)}$ and $\boldsymbol{X}'_{A,(k)}$. $PEP_{A,k}$ can be upper bounded as

$$PEP_{A,k} \leq \frac{8\sigma_B^4}{G_1 G_2 (s_k^4 - f_k^4)} \log\left(1 + \frac{G_1}{4\sigma_B^2}\sqrt{s_k^4 - f_k^4}\right) \times \log\left(1 + \frac{G_2}{4\sigma_B^2}\sqrt{s_k^4 - f_k^4}\right), \quad (15)$$

where

$$f_k^2 = \left| \sum_{m=BD_{\mathrm{AB}}+1}^{M} (X^{(m)}_{A,k} - X'^{(m)}_{A,k})(X^{(m-BD_{\mathrm{AB}})}_{A,k} - X'^{(m-BD_{\mathrm{AB}})}_{A,k})^* \right|,$$

$s_k^2 = \sum_{m=1}^{M} \left| X^{(m)}_{A,k} - X'^{(m)}_{A,k} \right|^2$ as in [9] and σ_B^2 is the noise variance at user B. For ANC-HD relaying, more time-domain noise samples will be accumulated due to the CA procedure which as a result will cause the frequency-domain samples to be correlated. However, to make the analysis tractable, we approximate $V^{(m)}_{B,k}$, $k \in \{1,2,\ldots,N\}$ in (7) by i.i.d. Gaussian random variables with zero mean and variance of $\sigma_B'^2 = \frac{\sigma_B^2}{N}(l_a N_N + N - N_N^2 N)$. Our simulation results fully corroborate this approximation as will be shown in the next section. Note that the noise variance is greater in case of the ANC-HD scheme, which explains the small performance degradation of ANC-HD relaying compared to ANC-FD relaying as discussed in Section V. Substituting $\sigma_B'^2$ in place of σ_B^2 in (15) provides an upper bound of the PEP of the ANC-HD scheme.

B. Independent Block Fading Frequency-Selective Channels

In an independent block fading scenario, the multipath channel gains remain fixed within each OFDM block and change independently from one block to the next. Hence, the multipath channel taps are independent across both delays and OFDM words. Without loss of generality, we assume $P_A = 1$, $G_1 = G_2 = 1$, and analyze the PEP by following a similar approach to the one in [9], [16]. Note that the channel model adopted considers independent block fading rather than the specific type of correlated block fading models used in [9], [16].

Let $BI(n)$ be the index of the block that contains the nth sample. The independent block-fading channel model is characterized by $h^n_{ir,l} = \alpha^{(m)}_{ir,l}$, $l \in \{1,2,\ldots,L_{ir}\}$, and $h^n_{ri,l} = \beta^{(m)}_{ri,l}$, $l \in \{1,2,\ldots,L_{ri}\}$, where $m = BI(n)$. The random variables $\alpha^{(m)}_{ir,l}$ and $\beta^{(m)}_{ri,l}$ are independent circularly symmetric complex Gaussian random variables with zero mean and variance of $\sigma^2_{ir,l}$ and $\sigma^2_{ri,l}$, respectively. An upper bound on the PEP of the ANC-FD scheme is derived in the Appendix as

$$PEP_{A,k} \leq \frac{1}{2} \prod_{m=1}^{M+BD_{\mathrm{AB}}} \prod_{c=1}^{n_m} \left[\frac{4\sigma_B^2}{\lambda_{k,m,c}\theta_g^{k_g}} \left((-1)^{k_g} \left(\frac{4\sigma_B^2}{\lambda_{k,m,c}} \right)^{k_g - 1} \times \exp\left(\frac{4\sigma_B^2}{\lambda_{k,m,c}\theta_g^{k_g}} \right) Ei\left(-\frac{4\sigma_B^2}{\lambda_{k,m,c}\theta_g^{k_g}} \right) + \theta_g \delta(k_g - 2) \right) \right], \quad (16)$$

where $Ei(.)$ is the exponential integral function defined as $Ei(x) = -\int_{-x}^{\infty} \frac{e^{-t}}{t} dt$ the vector $[k_g, \theta_g]$ is given by

$$\begin{cases} \left[2, \sigma^2_{\kappa,k,m,c,1}\sigma^2_{\mu,k,m,1}\right], & \text{if } \sigma^2_{\kappa,k,m,c,1}\sigma^2_{\mu,k,m,1} \\ & \quad = \sigma^2_{\kappa,k,m,c,2}\sigma^2_{\mu,k,m,2}, \\ \left[1, \sigma^2_{\kappa,k,m,c,r_{nz}}\sigma^2_{\mu,k,m,r_{nz}}\right], & \text{else.} \end{cases}$$

The definitions of $\lambda_{k,m,c}$, $\sigma^2_{\mu,k,m,r}$, $\sigma^2_{\kappa,k,m,c,r}$, $r \in \{1,2\}$, along with other details in arriving at the upper bound in (16) are provided in the Appendix. For the ANC-HD scheme, the PEP bound of the ANC-FD case holds true if the noise variance is properly scaled as explained in Section IV-A.

C. Correlated Block Fading Frequency-Selective Channels

In this case, we assume that the time-domain channel coefficients remain constant within each OFDM block and change from one block to another. Further, we assume that the multipath channel taps are independent across delays (or lags) and correlated across blocks (from one block to another). The correlated block-fading channel model assumed here is similar to the one used in [9], [16]. Let $m = BI(n)$, the channels are expressed as $h^n_{ir,l} = h^{(m)}_{ir,l} = \sum_{p=-\frac{L_t-1}{2}}^{\frac{L_t-1}{2}} \alpha_{ir,l}[p] e^{j\frac{2\pi p(m-1)}{M}}$, and $h^n_{ri,l} = h^{(m)}_{ri,l} = \sum_{p=-\frac{L_t-1}{2}}^{\frac{L_t-1}{2}} \beta_{ri,l}[p] e^{j\frac{2\pi p(m-1)}{M}}$ where $h^{(m)}_{ir,l}$ and $h^{(m)}_{ri,l}$ are the channel gains affecting the mth block for the corresponding links. $\alpha_{ir,l}[p]$ and $\beta_{ri,l}[p]$ are independent circularly symmetric complex Gaussian random variables with zero mean and variance of $\frac{\sigma^2_{ir,l}}{L_t}$ and $\frac{\sigma^2_{ri,l}}{L_t}$, respectively. The number of the expansion terms, L_t, is given by $L_t = \lceil 2 f_d M T + 1 \rceil$ where f_d is the maximum Doppler frequency shift and T is the OFDM symbol period. Let $\boldsymbol{w}_f(k) = \left[1, e^{-j\frac{2\pi(k-1)}{N}}, \ldots, e^{-j\frac{2\pi(k-1)(L-1)}{N}}\right]^T$, $\boldsymbol{\alpha}_{Ar}(l) = \left[\alpha_{Ar,l}\left[-\frac{L_t-1}{2}\right], \ldots, \alpha_{Ar,l}\left[\frac{L_t-1}{2}\right]\right]^T$, $\boldsymbol{\beta}_{rB}(l) = \left[\beta_{rB,l}\left[-\frac{L_t-1}{2}\right], \ldots, \beta_{rB,l}\left[\frac{L_t-1}{2}\right]\right]^T$, $r \in \{1,2\}$ and define

$$\begin{aligned} \boldsymbol{q} &= [q_1, \ldots, q_{2LL_t}]^T \\ &= \Big[\left[\boldsymbol{\beta}^H_{1B}(1), \ldots, \boldsymbol{\beta}^H_{1B}(L)\right], \\ &\qquad \left[\boldsymbol{\beta}^H_{2B}(1), \ldots, \boldsymbol{\beta}^H_{2B}(L)\right] e^{j\frac{2\pi(k-1)}{N} d_{\mathrm{AB}}} \Big]^T. \end{aligned}$$

Further, let $\boldsymbol{q}_1 = [q_1, \ldots, q_{LL_t}]^H$ and $\boldsymbol{q}_2 = [q_{LL_t+1}, \ldots, q_{2LL_t}]^H$, $\boldsymbol{h}^{(m)}_{Ar} = [[h^{(m)}_{Ar,1}, h^{(m)}_{Ar,2}, \ldots, h^{(m)}_{Ar,L_{Ar}}], \mathbf{0}^T_{(L-L_{Ar})}]^T$, $r \in \{1,2\}$, $\boldsymbol{h}^{(m)}_{rB} = [[h^{(m)}_{rB,1}, h^{(m)}_{rB,2}, \ldots, h^{(m)}_{rB,L_{rB}}], \mathbf{0}^T_{(L-L_{rB})}]^T$. Also, define $\boldsymbol{H}_{ArB,k} = [H^{(1)}_{ArB,k}, H^{(2)}_{ArB,k}, \ldots, H^{(M)}_{ArB,k}]$, $H^{(m)}_{A1B,k} = H^{(m)}_{A1,k} \times H^{(m)}_{1B,k}$ and $H^{(m)}_{A2B,k} = H^{(m)}_{A2,k} H^{(m)}_{2B,k} e^{-j\frac{2\pi(k-1)d_{\mathrm{AB}}}{N}}$ where $H^{(m)}_{Ar,k} = \sum_{l=1}^{L} h^{(m)}_{Ar,l} e^{-j\frac{2\pi(k-1)(l-1)}{N}} = \boldsymbol{h}^{(m)^T}_{Ar} \boldsymbol{w}_f(k)$ and $H^{(m)}_{rB,k} = \sum_{l=1}^{L} h^{(m)}_{rB,l} e^{-j\frac{2\pi(k-1)(l-1)}{N}} = \boldsymbol{h}^{(m)^T}_{rB} \boldsymbol{w}_f(k)$. The PEP conditioned on the channel gains is upper bounded by the Chernoff bound as in (21) in the Appendix where $d^2(\boldsymbol{X}_{A,(k)}, \boldsymbol{X}'_{A,(k)}) = \sum_{m=1}^{M+BD_{\mathrm{AB}}} \left| H^{(m)}_{A1B,k} d^m_k + H^{(m)}_{A2B,k} d^{m-BD_{\mathrm{AB}}}_k \right|^2$ and $d^m_k = X^{(m)}_{A,k} - X'^{(m)}_{A,k}$. Define the following quantities:

$$\begin{aligned} \boldsymbol{d}_k(m) &= \left[d^m_k, d^{m-BD_{\mathrm{AB}}}_k\right]^T, \\ \boldsymbol{w}_t(m) &= \left[e^{-j2\pi M f_d T}, \ldots, 1, \ldots, e^{j2\pi M f_d T}\right]^T, \\ \boldsymbol{W}_t(m) &= \mathrm{Bdiag}\left\{\boldsymbol{w}_t(m), \ldots, \boldsymbol{w}_t(m)\right\}_{LL_t \times L}, \\ \boldsymbol{W}_{t,f}(m,k) &= \mathrm{Bdiag}\left\{\boldsymbol{W}_t(m)\boldsymbol{w}_f(k), \boldsymbol{W}_t(m)\boldsymbol{w}_f(k)\right\}, \\ \boldsymbol{W}_{\alpha,t}(m) &= \mathrm{Bdiag}\left\{\boldsymbol{w}_t(m), \ldots, \boldsymbol{w}_t(m)\right\}_{LL_t^2 \times LL_t}, \\ \boldsymbol{W}_{A,t}(m) &= \mathrm{Bdiag}\left\{\boldsymbol{W}_{\alpha,t}(m), \boldsymbol{W}_{\alpha,t}(m)\right\}, \\ \boldsymbol{A}_{Ar}(k) &= \mathrm{Bdiag}\Bigg\{\sum_{l=1}^{L} e^{-j\frac{2\pi(k-1)(l-1)}{N}} \boldsymbol{\alpha}^T_{Ar}(l), \ldots, \\ &\qquad \sum_{l=1}^{L} e^{-j\frac{2\pi(k-1)(l-1)}{N}} \boldsymbol{\alpha}^T_{Ar}(l)\Bigg\}_{LL_t \times LL_t^2}. \end{aligned}$$

By defining $\boldsymbol{q}(k) = [\boldsymbol{q}^T_1 \boldsymbol{A}_{A1}(k), \boldsymbol{q}^T_2 \boldsymbol{A}_{A2}(k)]^H$ and

$$\begin{aligned} \boldsymbol{D}_A(\boldsymbol{X}_k, \boldsymbol{X}'_k) = &\sum_{m=1}^{M+BD} \boldsymbol{W}_{A,t}(m) \boldsymbol{W}_{t,f}(m,k) \\ &\times \boldsymbol{d}_k(m) \boldsymbol{d}^H_k(m) \boldsymbol{W}^H_{t,f}(m,k) \boldsymbol{W}^H_{A,t}(m), \end{aligned}$$

we can express the squared distance as

$$d^2\left(\boldsymbol{X}_{A,(k)}, \boldsymbol{X}'_{A,(k)}\right) = \boldsymbol{q}(\boldsymbol{k})^H \boldsymbol{D}_A(\boldsymbol{X}_k, \boldsymbol{X}'_k) \boldsymbol{q}(k). \quad (17)$$

Since $\boldsymbol{D}_A(\boldsymbol{X}_k, \boldsymbol{X}'_k)$ is a positive semidefinite matrix, we can write

$$\boldsymbol{D}_A(\boldsymbol{X}_k, \boldsymbol{X}'_k) = \boldsymbol{U}_k \boldsymbol{\Lambda}_k \boldsymbol{U}^H_k, \quad (18)$$

where $\boldsymbol{U}_k$ is a unitary matrix and $\boldsymbol{\Lambda}_k = \mathrm{diag}\{\lambda_{k,1}, \ldots, \lambda_{k,n_k}, 0, \ldots, 0\}$ is the diagonal matrix whose diagonal elements are the eigenvalues of $\boldsymbol{D}_A(\boldsymbol{X}_k, \boldsymbol{X}'_k)$. Let $\boldsymbol{\mu}_r(k) = [\mu_{k,r,1}, \ldots, \mu_{k,r,L_t}] = \sum_{l=1}^{L} e^{-j\frac{2\pi(k-1)(l-1)}{N}} \boldsymbol{\alpha}_{Ar}(l)$ and

$$\chi_{k,c,p} = \sum_{t=1}^{L_t} U^*_{k,c,(p-1)L_t+(p-1)L_t+t} \mu_{k,\left\lfloor \frac{p-1}{LL_t}+1 \right\rfloor, t}$$

where $\boldsymbol{U}_{k,c}$ denotes the cth column of $\boldsymbol{U}_k$ with $U_{k,c,p}$ being the pth element in $\boldsymbol{U}_{k,c}$, we can further write the squared distance as

$$d^2\left(\boldsymbol{X}_{A,(k)}, \boldsymbol{X}'_{A,(k)}\right) = \sum_{c=1}^{n_k} \lambda_{k,c} \left| \sum_{p=1}^{2LL_t} q_p \chi_{k,c,p} \right|^2, \quad (19)$$

where q_p and $\chi_{k,c,p}$ are assumed to be independent complex Gaussian random variables with zero mean and variance of $\sigma^2_{q,p}$ and

$$\sigma^2_{\chi,k,(i-1)LL_t+p} = \sum_{l=1}^{L} \sigma^2_{h_{Ar},l} \sum_{t=1}^{L_t} \left| U_{k,c,(i-1)LL_t^2+(p-1)L_t+t} \right|^2,$$

respectively. The approximate PEP upper bound for the ANC-FD scheme assuming $P_A = 1$ and $G_1 = G_2 = 1$ is given in (20), shown at the bottom of the next page, where $\pi_p = \prod_{l \in S_0, l \neq p} \frac{\sigma^2_{\chi,k,p}\sigma^2_{q,p}}{\sigma^2_{\chi,k,p}\sigma^2_{q,p} - \sigma^2_{\chi,k,l}\sigma^2_{q,l}}$ and S_0 refers to the set of distinct values of $\sigma^2_{\chi,k,p}\sigma^2_{q,p}$. S_j, $j \in \{1, 2, \ldots, J\}$, refers to the set for which j of the terms $\sigma^2_{\chi,k,p}\sigma^2_{q,p}$ are equal.

TABLE I
SIMULATION PARAMETERS

Parameter	Value(s)	
	Figs. 10.a and 11	Figs. 12 and 13
M	10	10
N	64	64
BW	3 kHz	8 kHz
$\{\sigma_{ir,l}\}_{l\in\{1,2,\ldots,L_{ir}\}}$ $i\in\{A,B\}$, $r\in\{1,2\}$	UWA-like sparse channels[a]	$\frac{[1,\ 0.8,\ 0.6]}{\sqrt{2}}$
D_{A1}	0	0
D_{B1}	48	48
D_{A2}	0	0
D_{B2}	56	56
D_{1B}	0	0
D_{2B}	286	145

[a] The sparse channels generated have a maximum delay spread of 20 ms (equivalent to 60 sample times) defined by $\{\sigma_{ir,l}\}_{l\in\{1,2,\ldots,L_{ir}\}} = [0.6667, 0.4000, 0.5333, 0.2667, 0.2000]$, $i\in\{A,B\}$, $r\in\{1,2\}$, taking place on the lags $[1.67\,ms,\ 2.67\,ms,\ 3.67\,ms,\ 7\,ms,\ 20\,ms]$, respectively.

As in [9], we make the following assumptions: (A) pairwise independence among q_p, $p\in\{1,2,\ldots,2LL_t\}$, (B) pairwise independence among $\chi_{k,c,p}$, $p\in\{1,2,\ldots,LL_t\}$ and (C) independence between q_p and $\chi_{k,c,p'}$, $p\in\{1,2,\ldots,2LL_t\}$ and $p'\in\{1,2,\ldots,2LL_t\}$. While (A) and (C) are certainly valid, (B) is only an approximation.

V. NUMERICAL RESULTS AND DISCUSSION

In this section, we investigate the performance of the proposed schemes through simulations and numerical calculations of the analytical results. We employ an OFDM modulator with N subcarriers over a total bandwidth of BW. The SNR at user i while aiming to estimate the signal of user i' is defined as

$$SNR_i = \frac{(G_1+G_2)P_{i'}}{\sigma^2_{i,eff}}, \quad i,i'\in\{A,B\},\ i'\neq i$$

where $\sigma^2_{i,eff} = G_1\sigma_1^2 + G_2\sigma_2^2 + \sigma_i^2$ is the effective noise variance at user i after accounting for the amplified noise terms at the relays (due to ANC). We consider Rayleigh multipath fading channels with different assumptions on time variability. Unless stated otherwise, we assume that the channels undergo quasi-static fading, Quadrature PSK (QPSK) modulation is used, and $\sigma_B^2 = \sigma_1^2 = \sigma_2^2$. We further assume that $P_A = 1$ and $G_1 = G_2 = 1$. Table I lists some of the simulation parameters pertaining to each figure. In Figs. 10 and 11, we compare the proposed ANC-FD and ANC-HD schemes with the ANC-STBC scheme in [5] which is to our knowledge the best result reported in the literature of asynchronous DTWR systems in terms of bit error rates (BERs). We also compare our results to the ANC-OFDM scheme based on [2]. To ensure a fair comparison, our simulation uses the same number of relays ($N_R = 2$) and the same assumptions for the channels in all the schemes. We also impose equal power and rate to guarantee fairness in terms of power, temporal and spectral resources.

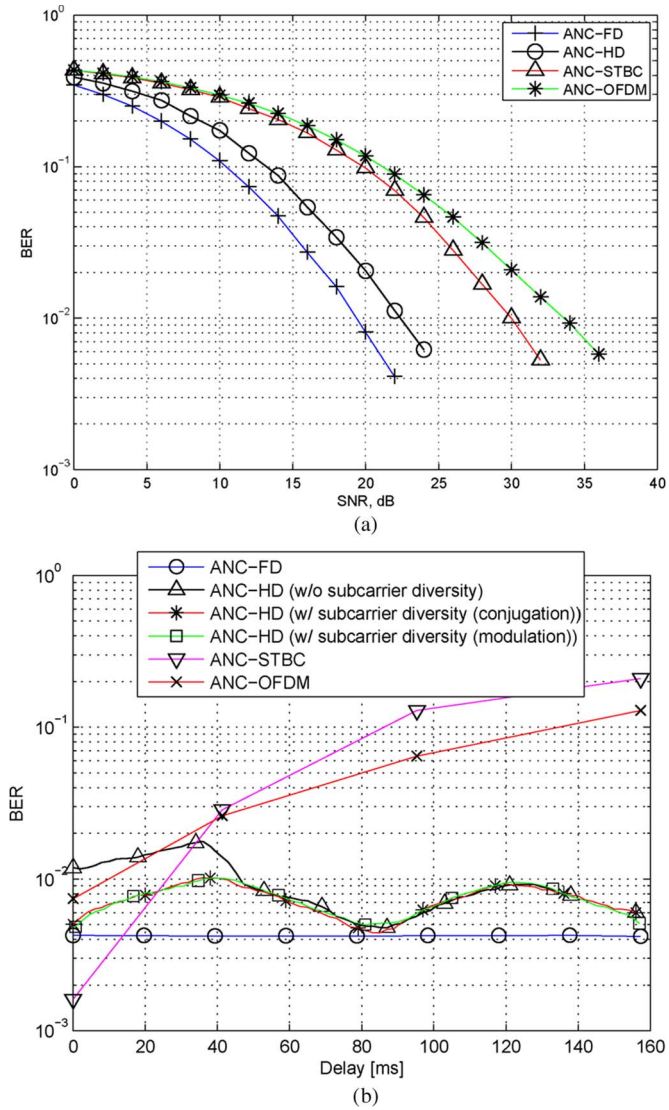

Fig. 10. Comparison of the BER performance between the proposed ANC-HD scheme and two existing schemes [2], [5] with imposing an equal rate criteria ($M = 10$ and $N = 64$). (a) Fixed delay of 286 samples. (b) Fixed SNR of 24 dB.

$$PEP_{A,k} \overset{\sim}{<} \frac{1}{2}\prod_{c=1}^{n_k}\left(\sum_{p\in S_0}\frac{\pi_p}{\sigma^2_{\chi,k,p}\sigma^2_{q,p}}\frac{2\sigma_B^2}{\lambda_{k,c}}\exp\left(\frac{2\sigma_B^2}{\lambda_{k,c}\sigma^2_{\chi,k,p}\sigma^2_{q,p}}\right)Ei\left(\frac{2\sigma_B^2}{\lambda_{k,c}\sigma^2_{\chi,k,p}\sigma^2_{q,p}}\right)+\sum_{j=1}^{J}\sum_{p\in S_j}\frac{\left(2\sigma_B^2\right)^{N_j}(-1)^{N_j-1}}{(N_j-1)!\left(\lambda_{k,c}\sigma^2_{\chi,k,p}\sigma^2_{q,p}\right)^{N_j}}\right.$$
$$\left.\times\left[\exp\left(\frac{2\sigma_B^2}{\lambda_{k,c}\sigma^2_{\chi,k,p}\sigma^2_{q,p}}\right)Ei\left(\frac{2\sigma_B^2}{\lambda_{k,c}\sigma^2_{\chi,k,p}\sigma^2_{q,p}}\right)+\sum_{k=1}^{N_j-1}(k-1)!\left(\frac{-\lambda_{k,c}\sigma^2_{\chi,k,p}\sigma^2_{q,p}}{2\sigma_B^2}\right)^k\right]\right) \quad (20)$$

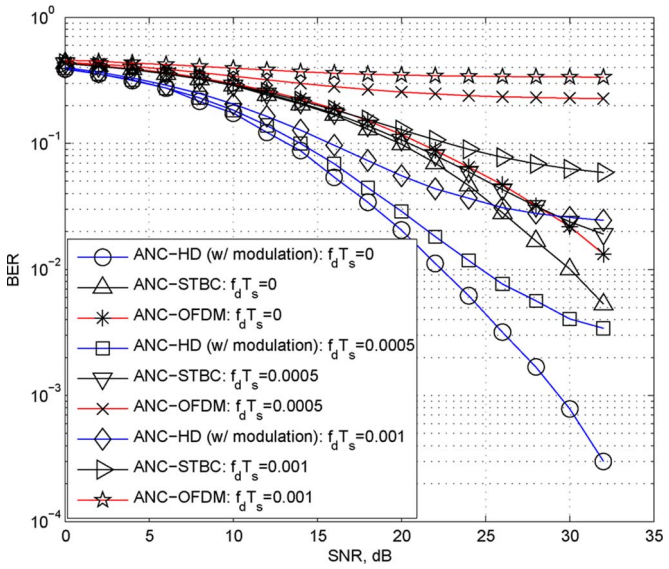

Fig. 11. Comparison of the BER performance between the proposed ANC-HD scheme and two existing schemes [2], [5] for various fade rates.

For the ANC-STBC and ANC-OFDM schemes, longer CP is required while experiencing larger delays and hence we increase the size of their constellations to maintain the same rate as our schemes (refer to Section III-B4 for the data rate expressions). For the duplexing method, the schemes in [2], [5] use half-duplex nodes while our proposed scheme uses full-duplex users and either half- or full-duplex relays and hence our schemes have an increased hardware complexity.

Fig. 10(a) compares the average BER of our ANC-FD and ANC-HD schemes with both the ANC-STBC and ANC-OFDM schemes. With the parameters in Table I, the minimum CP length for ANC-STBC and ANC-OFDM at each phase is 346 samples, which means that the effective transmission of $N = 64$ data samples using either ANC-STBC or ANC-OFDM requires 820 samples. On the other hand, for ANC-FD and ANC-HD scenarios, the minimum CP length is only 184 as it is independent from the delay. Moreover, the effective delay is $D_{\rm AB} = 286$ samples (equivalent to 95.334 ms) which means that we have one block delay, i.e., $BD_{\rm AB} = 1$ and the residual delay $d_{\rm AB} = 38$ samples. We impose an equal rate condition on the four schemes, and as a result, the ANC-HD scheme, for instance, outperforms both ANC-STBC and ANC-OFDM by about 7.5 dB and 10.5 dB, respectively, at a BER of about 10^{-2}. Alternatively, without imposing an equal rate criterion, the performances of all the above schemes are comparable, which means that the proposed solutions can transmit at a higher rate without sacrificing the performance.

To illustrate the advantages of having the CP length independent from the delay, we plot in Fig. 10(b) the BER versus the delay $(D_{\rm AB})$. Herein, the simulation parameters are similar to those used for Fig. 10(a) except that we set a fixed SNR of 24 dB and vary D_{2B} from 0 to 480. Clearly, the performances of ANC-STBC and ANC-OFDM suffer greatly due to the increase in relative delay while the ANC-HD scheme shows robustness against asynchrony. On the other hand, the ANC-FD scheme shows further robustness against asynchrony since its performance is unaffected by the increase in relative delay. For instance, at a delay of 160 ms (which may be observed in UWA communications [17]), a performance improvement of about two orders of magnitude in the error rate is observed. It is also noted that ANC-STBC performs better than the ANC-FD scheme for small delay values (less than 15 ms and 25 ms for ANC-FD and ANC-HD, respectively). We also show in Fig. 10(b) the effect of applying the subcarrier diversity scheme in improving the performance for small delays.

In Fig. 11, we compare the ANC-HD scheme to ANC-STBC and ANC-OFDM under a time-varying fading scenario with various fade rates. The time-varying fading channel is generated using Jakes' model, i.e., the sum of sinusoids method [18]. We can see that the ANC-HD scheme is the most resilient solution to temporal variations of the channel even without performing frequency domain equalization. An error floor, however, is inevitable for this case due to neglecting the ICI in the off-diagonal elements of $H_{sc,ArB}$.

We next evaluate and discuss our analytical findings for the PEP. We first define the Hamming distance $D(\boldsymbol{X}_{A,(k)}, \boldsymbol{X}'_{A,(k)})$, or D for short, between two sequences $\boldsymbol{X}_{A,(k)}$ and $\boldsymbol{X}'_{A,(k)}$ for our system as the number of instances at which either the symbols from the first relay or the delayed symbols from the second relay are different. It can be evaluated as $D = \sum_{m=1}^{M+BD_{\rm AB}} I_{k,m}$, where

$$I_{k,m} = \begin{cases} 1, & X_{A,k}^{(m)} \neq X_{A,k}^{\prime(m)} \text{ or } X_{A,k}^{(m-BD_{\rm AB})} \neq X_{A,k}^{\prime(m-BD_{\rm AB})}, \\ 0, & \text{otherwise}, \end{cases}$$

and $X_{A,k}^{(m)} = X_{A,k}^{\prime(m)} = 0$ if $m < 1$ or $m > M + BD_{\rm AB}$. For Fig. 12, we discard the noise at the relays and study the PEP for a specific subcarrier index. We further assume one-block delay with residual delay $d_{\rm AB} = 11$. We choose $\boldsymbol{X}_{A,(k)} = \mathbf{1}_{10}$ as a reference sequence. Fig. 12(a) compares the analytical upper bound for the PEP for the ANC-FD scheme to the estimated PEP obtained from Monte Carlo calculations under correlated block fading channel conditions with $f_d T_s = 0.01$. We compare two cases of the Hamming distance, namely 2 and 4 corresponding to $\boldsymbol{X}'_{A,(k)} = [-1, \mathbf{1}_9^T]^T$ and $\boldsymbol{X}'_{A,(k)} = [-1, \mathbf{1}_8^T, -1]^T$ respectively. We compare two cases of the Hamming distance, namely 2 and 4 as defined above. The effects assuming independence of different $\chi_{k,c,p}$ values are shown in Fig. 12(a) where we compare the simulation results that represent the estimated value of the PEP to the Chernoff bound evaluated for two cases; correlated $\chi_{k,c,p}$ and independent $\chi_{k,c,p}$. As seen in the figure, the evaluation of the Chernoff bound when $\chi_{k,c,p}$ is correlated (according to the channel model in Section IV-C) agrees with the simulation results. However, when we generate independent $\chi_{k,c,p}$, the results are only approximate, but even though, the bound can be used to study the diversity order or to design channel codes.

In Fig. 12(b), we consider an ANC-HD system and compare the theoretical PEP upper bound to the estimated PEP under independent block fading conditions. We consider an additional value of $D(\boldsymbol{X}_{A,(k)}, \boldsymbol{X}'_{A,(k)}) = 6$ that corresponds to $\boldsymbol{X}'_{A,(k)} = [-\mathbf{1}_5^T, \mathbf{1}_5^T]^T$. Fig. 12(b) clearly shows the tightness of the derived bound.

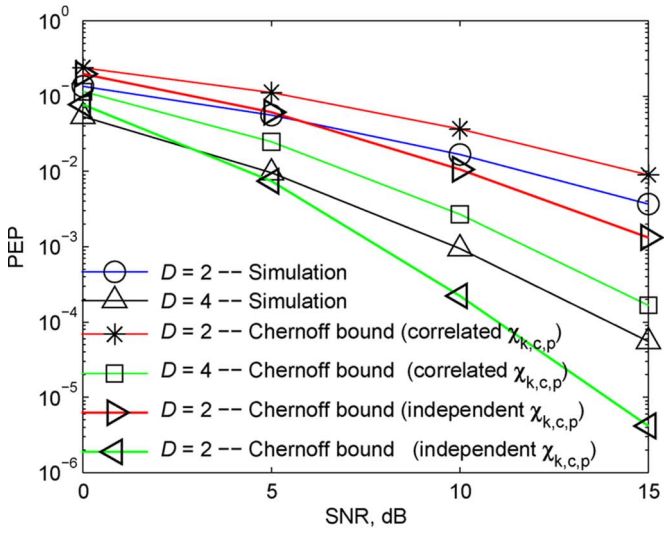

(a)

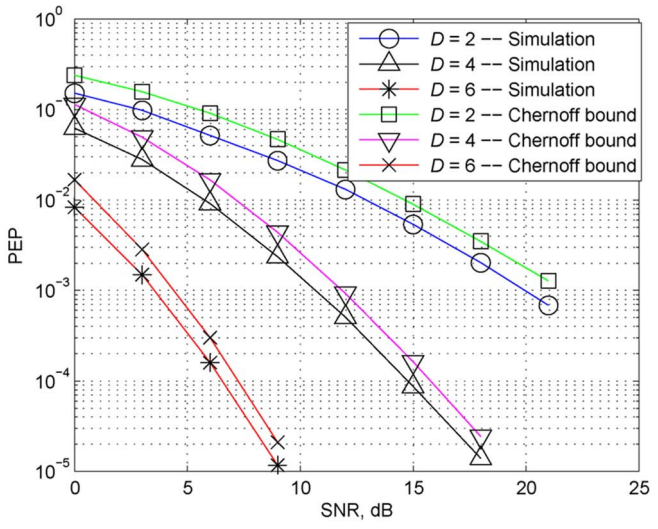

(b)

Fig. 12. Comparison between the PEP upper bound and the estimated PEP performance for various values of the Hamming distance. For this figure, $M = 10$ and $k = 15$. (a) Correlated block fading channel (ANC-FD). (b) Independent block fading channel (ANC-HD).

Finally, we comment on the effects of estimation errors in propagation delays on the performance. Even though proper operation of the proposed schemes is heavily dependent on the accurate knowledge of the delays, our application of UWA communications only requires the estimation accuracy to be in the range of tenths of a millisecond. For example, for an OFDM system with a total occupied bandwidth of 3 kHz (over the frequency band: 12 kHz–15 kHz) with $N = 64$ subcarriers, the delay estimation error should not exceed 0.167 ms which is half the sampling time. This accuracy is achievable with the current state of art, for instance, as shown in [19]. On the other hand, our schemes show robustness against errors in channel gain estimation. We demonstrate this point by corrupting the channel gain at time n and lag l, i.e. $h^n_{ir,l}$, $i, r \in \{A, B, 1, 2\}$, $i \neq r$, by a complex Gaussian noise with zero mean and variance $\sigma^2_{est,n,ir,l}$. Define the relative estimation error, ϵ_{est}, by $\epsilon_{est} = \frac{\sigma_{est,n,ir,l}}{|h^n_{ir,l}|}$. Fig. 13 shows the effect of different levels of the

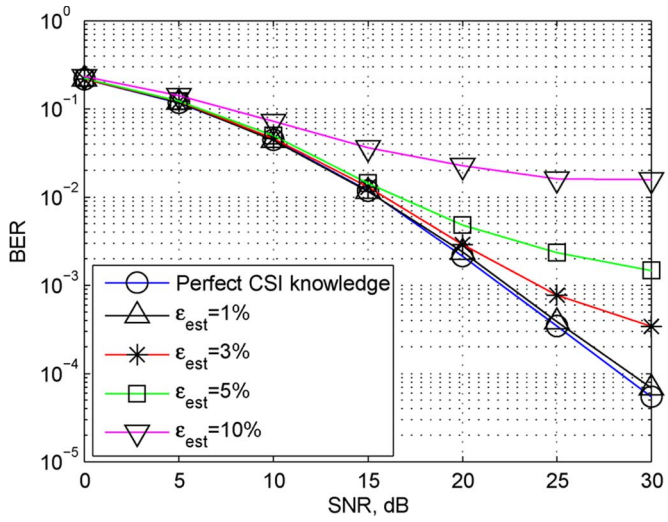

Fig. 13. Effect of the estimation error on the BER for quasi-static fading channels.

estimation error on the BER for the ANC-HD scheme (similar behavior is observed for the ANC-FD scheme). Clearly, for this example, when the estimation error is up to 5%, there is almost no loss in the performance for SNR values below 15 dB compared to the case of perfect CSI estimation. For higher levels of the estimation error, the loss increases gradually. We observed similar behaviour with time-varying fading.

VI. Conclusion

We have considered an asynchronous dual-relay TWR system in doubly selective fading channels with large relative delays such as those observed in UWA communications. We have proposed two spectrally-efficient OFDM-based schemes in which the minimum cyclic-prefix length is independent of the relative propagation delays experienced. An important aspect of the proposed schemes is that they not only solve the large delay problem but also enhance the error rate performance by exploiting the inherent delay diversity in the signal structure. Through Monte Carlo simulations and analytical PEP evaluations, we have verified our findings and showed the advantages of the proposed schemes compared to existing ones in the literature. Among the proposed schemes, the ANC-FD scheme offers the best performance while the ANC-HD scheme may be a more practical solution due to the use of half-duplex relays.

Appendix A
PEP Analysis for Independent Block Fading Frequency-Selective Channels

Let $\boldsymbol{\alpha}^{(m)}_{Ar} = [[\alpha^{(m)}_{Ar,1}, \alpha^{(m)}_{Ar,2}, \ldots, \alpha^{(m)}_{Ar,L_{Ar}}], \mathbf{0}^T_{(L-L_{Ar})}]^T$, $r \in \{1, 2\}$, $\boldsymbol{\beta}^{(m)}_{1B} = [[\beta^{(m)}_{1B,1}, \beta^{(m)}_{1B,2}, \ldots, \beta^{(m)}_{1B,L_{1B}}], \mathbf{0}^T_{(L-L_{1B})}]^T$, $\boldsymbol{\beta}^{(m)}_{2B} = [[\beta^{(m)}_{2B,1}, \beta^{(m)}_{2B,2}, \ldots, \beta^{(m)}_{2B,L_{2B}}], \mathbf{0}^T_{(L-L_{2B})}]^T e^{-j\frac{2\pi(k-1)d_{AB}}{N}}$, and $\boldsymbol{w}_f(k) = [1, e^{-j\frac{2\pi(k-1)}{N}}, \ldots, e^{-j\frac{2\pi(k-1)(L-1)}{N}}]^T$. Also, define $\boldsymbol{H}_{ArB,k} = [H^{(1)}_{ArB,k}, H^{(2)}_{ArB,k}, \ldots, H^{(M)}_{ArB,k}]$ and $H^{(m)}_{ArB,k} = H^{(m)}_{Ar,k} \times H^{(m)}_{rB,k}$ where $H^{(m)}_{Ar,k} = \sum_{l=1}^{L} \alpha^{(m)}_{Ar,l} e^{-j\frac{2\pi(k-1)(l-1)}{N}} = \boldsymbol{\alpha}^{(m)T}_{Ar} \times \boldsymbol{w}_f(k)$ and $H^{(m)}_{rB,k} = \sum_{l=1}^{L} \beta^{(m)}_{rB,l} e^{-j\frac{2\pi(k-1)(l-1)}{N}} = \boldsymbol{\beta}^{(m)T}_{rB} \boldsymbol{w}_f(k)$.

Using the Chernoff bound, the PEP conditioned on known channel conditions can be upper bounded as

$$P\left(\boldsymbol{X}_{A,(k)} \rightarrow \boldsymbol{X}'_{A,(k)} | \boldsymbol{H}_{ArB,k},\ r \in \{1,2\}\right) \leq \frac{1}{2} e^{-\frac{d^2\left(\boldsymbol{X}_{A,(k)}, \boldsymbol{X}'_{A,(k)}\right)}{4\sigma_B^2}}, \quad (21)$$

where the squared distance $d^2(\boldsymbol{X}_{A,(k)}, \boldsymbol{X}'_{A,(k)}) = \sum_{m=1}^{M+BD_{\mathrm{AB}}} \left| H^{(m)}_{A1B,k} d^m_k + H^{(m)}_{A2B,k} d^{m-BD_{\mathrm{AB}}}_k \right|^2$ and $d^m_k = X^{(m)}_{A,k} - X'^{(m)}_{A,k}$. Expanding $H^{(m)}_{ArB,k}$, the squared distance can be written as

$$d^2\Big(\boldsymbol{X}_{A,(k)}, \boldsymbol{X}'_{A,(k)}\Big) = \sum_{m=1}^{M+BD_{\mathrm{AB}}} \boldsymbol{w}_f^T(k) \left[\boldsymbol{\alpha}^{(m)}_{A1} \boldsymbol{\beta}^{(m)^T}_{1B}, \boldsymbol{\alpha}^{(m)}_{A2} \boldsymbol{\beta}^{(m)^T}_{2B}\right] \boldsymbol{W}_f(k) \boldsymbol{d}_k(m) \times \boldsymbol{d}^H_k(m) \boldsymbol{W}^H_f(k) \left[\boldsymbol{\alpha}^{(m)}_{A1} \boldsymbol{\beta}^{(m)^T}_{1B}, \boldsymbol{\alpha}^{(m)}_{A2} \boldsymbol{\beta}^{(m)^T}_{2B}\right]^H \boldsymbol{w}^*_f(k), \quad (22)$$

where $\boldsymbol{W}_f(k) = \mathrm{Bdiag}\{\boldsymbol{w}_f(k), \boldsymbol{w}_f(k)\}$ and $\boldsymbol{d}_k(m) = [d^m_k, d^{m-BD_{\mathrm{AB}}}_k]^T$. Let $D^{(m)}_A(\boldsymbol{X}_{A,(k)}, \boldsymbol{X}'_{A,(k)}) = \boldsymbol{W}_f(k) \boldsymbol{d}_k(m) \times \boldsymbol{d}^H_k(m) \boldsymbol{W}^H_f(k)$ and $\mu^{(m)^*}_{k,r} = \sum_{l=1}^{L} e^{-j\frac{2\pi(k-1)(l-1)}{N}} \alpha^{(m)}_{Ar,l}$, $r \in \{1,2\}$. Noting that

$$\boldsymbol{w}_f^T(k) \left[\boldsymbol{\alpha}^{(m)}_{A1} \boldsymbol{\beta}^{(m)^T}_{1B}, \boldsymbol{\alpha}^{(m)}_{A2} \boldsymbol{\beta}^{(m)^T}_{2B}\right] = \left[\boldsymbol{\beta}^{(m)^T}_{1B} \sum_{l=1}^{L} e^{-j\frac{2\pi(k-1)(l-1)}{N}} \alpha^{(m)}_{A1,l}, \boldsymbol{\beta}^{(m)^T}_{2B} \sum_{l=1}^{L} e^{-j\frac{2\pi(k-1)(l-1)}{N}} \alpha^{(m)}_{A2,l}\right],$$

we can write

$$d^2\left(\boldsymbol{X}_{A,(k)}, \boldsymbol{X}'_{A,(k)}\right) = \sum_{m=1}^{M+BD_{\mathrm{AB}}} \boldsymbol{q}(k,m)^H D^{(m)}_A\left(\boldsymbol{X}_{A,(k)}, \boldsymbol{X}'_{A,(k)}\right) \boldsymbol{q}(k,m),$$

where $\boldsymbol{q}(k,m) = [\mu^{(m)}_{k,1}\ \boldsymbol{\beta}^{(m)^H}_{1B}, \mu^{(m)}_{k,2}\ \boldsymbol{\beta}^{(m)^H}_{2B}]^T$. Since the matrix $D^{(m)}_A(\boldsymbol{X}_{A,(k)}, \boldsymbol{X}'_{A,(k)})$ is Hermitian, then it is diagonalizable. Therefore, we can write $D^{(m)}_A(\boldsymbol{X}_{A,(k)}, \boldsymbol{X}'_{A,(k)}) = \boldsymbol{U}_{k,m} \boldsymbol{\Lambda}_{k,m} \boldsymbol{U}^H_{k,m}$, where $\boldsymbol{U}_{k,m}$ is a unitary matrix and $\boldsymbol{\Lambda}_{k,m} = \mathrm{diag}\{\lambda_{k,m,1}, \ldots, \lambda_{k,m,n_m}, 0, \ldots, 0\}$ where $\{\lambda_{k,m,i}\}_{i=1}^{n_m}$ are the positive eigenvalues of $D^{(m)}_A(\boldsymbol{X}_{A,(k)}, \boldsymbol{X}'_{A,(k)})$.[1] Note that $D^{(m)}_A(\boldsymbol{X}_{A,(k)}, \boldsymbol{X}'_{A,(k)})$ is not affected by the channel coefficients; it only depends on the code structure. Having that established, we can now rewrite the squared distance as

$$d^2\Big(\boldsymbol{X}_{A,(k)}, \boldsymbol{X}'_{A,(k)}\Big) = \sum_{m=1}^{M+BD_{\mathrm{AB}}} \sum_{c=1}^{n_m} \lambda_{k,m,c} \left|\boldsymbol{U}^H_{k,m,c} \boldsymbol{q}(k,m)\right|^2, \quad (23)$$

where $\boldsymbol{U}_{k,m,c}$ is the cth column of $\boldsymbol{U}_{k,m}$. Note that we can expand $U^H_{k,m,c} \boldsymbol{q}(k,m)$ as

$$U^H_{k,m,c} \boldsymbol{q}(k,m) = \sum_{l=1}^{L} U^*_{k,m,c,l} \mu^{(m)}_{k,1} \beta^{(m)^*}_{1B,l} + \sum_{l=1}^{L} U^*_{k,m,c,L+l} \mu^{(m)}_{k,2} \beta^{(m)^*}_{2B,l} e^{j\frac{2\pi(k-1)d_{\mathrm{AB}}}{N}}, \quad (24)$$

where $\boldsymbol{U}_{k,m,c,l}$ denotes the lth element of $\boldsymbol{U}_{k,m,c}$.

Let $\kappa^{(m)}_{k,c,1} = \sum_{l=1}^{L} U^*_{k,m,c,l} \beta^{(m)^*}_{1B,l}$ and $\kappa^{(m)}_{k,c,2} = \sum_{l=1}^{L} U^*_{k,m,c,L+l} \beta^{(m)^*}_{2B,l} e^{j\frac{2\pi(k-1)d_{\mathrm{AB}}}{N}}$. Now, we can rewrite (23) as

$$d^2\left(\boldsymbol{X}_{A,(k)}, \boldsymbol{X}'_{A,(k)}\right) = \sum_{m=1}^{M+BD_{\mathrm{AB}}} \sum_{c=1}^{n_m} \lambda_{k,m,c} \left|\sum_{r=1}^{2} \mu^{(m)}_{k,r} \kappa^{(m)}_{k,c,r}\right|^2, \quad (25)$$

Note that the term $\left|\sum_{r=1}^{2} \mu^{(m)}_{k,r} \kappa^{(m)}_{k,c,r}\right|^2$ is correlated across different values of c that correspond to different Eigen values because for a fixed value of the pair $\{m,r\}$ and different c values, $\mu^{(m)}_{k,r}$ is the same and $\kappa^{(m)}_{k,c,r}$ is a linear combination of the same L i.i.d. random variables $\beta^{(m)^*}_{rB,l}$. However, By examining the correlation coefficients, we have found that they are negligible. Hence, we consider them independent to simplify the analysis. The validity of this assumption has been supported by the Monte Carlo simulation of the PEP in Section V. Now, we can write

$$PEP_{A,k} \leq \frac{1}{2} E_{\substack{\boldsymbol{H}_{ArB,k} \\ r\in\{1,2\}}} \left[\exp\left(-\frac{1}{4\sigma_B^2} \sum_{m=1}^{M+BD_{\mathrm{AB}}} \sum_{c=1}^{n_m} \lambda_{k,m,c} \times \left|\sum_{r=1}^{2} \mu^{(m)}_{k,r} \kappa^{(m)}_{k,c,r}\right|^2\right)\right], \quad (26)$$

To evaluate the PEP upper bound in (28), shown at the bottom of the next page, we assume that $\mu^{(m)}_{k,r}$ and $\kappa^{(m)}_{k,c,r}$, $\forall r \in \{1,2\}$ and $\forall m \in \{1, \ldots, M+BD_{\mathrm{AB}}\}$, are independent complex Gaussian random variables with zero mean and variance of $\sigma^2_{\mu,k,m,r} = \sum_{l=1}^{L} \sigma^2_{h_{Ar},l}$ and $\sigma^2_{\kappa,k,m,c,r} = \sum_{l=1}^{L} |U_{k,m,c,(r-1)L+l}|^2 \sigma^2_{h_{rB},l}$ respectively. Hence, we may write

$$E_{\substack{\boldsymbol{H}_{ArB,k} \\ r\in\{1,2\}}} \left[\exp\left(-\frac{1}{4\sigma_B^2} \sum_{m=1}^{M+BD_{\mathrm{AB}}} \sum_{c=1}^{n_m} \lambda_{k,m,c} \left|\sum_{r=1}^{2} \mu^{(m)}_{k,r} \kappa^{(m)}_{k,c,r}\right|^2\right)\right] = \prod_{m=1}^{M+BD_{\mathrm{AB}}} \prod_{c=1}^{n_m} PEP_{k,m,c}, \quad (27)$$

[1] Note that the matrix $D^{(m)}_A(\boldsymbol{X}_{A,(k)}, \boldsymbol{X}'_{A,(k)})$ is positive semidefinite due to having the structure $A^H A$ where $A = d^H_k(m) \boldsymbol{W}^H_f(k)$.

where

$$PEP_{k,m,c}=E_{\substack{\mu_{k,r}^{(m)},\kappa_{k,c,r}^{(m)}\\ r\in\{1,2\}}}\left[\exp\left(-\frac{1}{4\sigma_B^2}\lambda_{k,m,c}\left|\sum_{r=1}^{2}\mu_{k,r}^{(m)}\kappa_{k,c,r}^{(m)}\right|^2\right)\right].$$

By writing $\mu_{k,r}^{(m)}\kappa_{k,c,r}^{(m)}$ as $\mu_{k,r}^{(m)}\kappa_{k,c,r}^{(m)}=|\mu_{k,r}^{(m)}\kappa_{k,c,r}^{(m)}|\angle\phi_{k,c,r}^{(m)}$ and $\sum_{r=1}^{2}\mu_{k,r}^{(m)}\kappa_{k,c,r}^{(m)}$ as $\sum_{r=1}^{2}\mu_{k,r}^{(m)}\kappa_{k,c,r}^{(m)}=|\sum_{r=1}^{2}\mu_{k,r}^{(m)}\times\kappa_{k,c,r}^{(m)}|\angle\theta_{k,c}^{(m)}$, we can expand the term $|\sum_{r=1}^{2}\mu_{k,r}^{(m)}\kappa_{k,c,r}^{(m)}|^2$ as

$$\left|\sum_{r=1}^{2}\mu_{k,r}^{(m)}\kappa_{k,c,r}^{(m)}\right|^2=2\left|\mu_{k,1}^{(m)}\kappa_{k,c,1}^{(m)}\right|\left|\mu_{k,2}^{(m)}\kappa_{k,c,2}^{(m)}\right|\times\cos\left(\phi_{k,c,1}^{(m)}-\theta_{k,c}^{(m)}\right)+\sum_{r=1}^{2}\left|\mu_{k,r}^{(m)}\kappa_{k,c,r}^{(m)}\right|^2 \quad (29)$$

The problem of finding the PEP bound reduces to evaluating the expectation in (26) over the set of random variables $S=\{|\mu_{k,1}^{(m)}|,|\mu_{k,2}^{(m)}|,|\kappa_{k,c,1}^{(m)}|,|\kappa_{k,c,2}^{(m)}|,\phi_{k,c,1}^{(m)},\theta_{k,c}^{(m)}\}$. Let $S\setminus R$ denote the relative compliment of R in S which is the set of all elements in S that are not in R. To obtain the PEP, we sequentially integrate over the elements of S using the law of total expectation. Since $\phi_{k,c,r}^{(m)}$ and $\theta_{k,c}^{(m)}$ are by assumption i.i.d. Uniform random variables over $[0,2\pi]$, then

$$\begin{aligned}PEP_{k,m,c}&=E_S\left[\exp\left(-\frac{1}{4\sigma_B^2}\lambda_{k,m,c}\left|\sum_{r=1}^{2}\mu_{k,r}^{(m)}\kappa_{k,c,r}^{(m)}\right|^2\right)\right]\\&=E_{S\setminus\left\{\phi_{k,c,1}^{(m)}\right\}}\left[E_{\phi_{k,c,1}^{(m)}/S\setminus\left\{\phi_{k,c,1}^{(m)}\right\}}\left[\exp\left(-\frac{1}{4\sigma_B^2}\lambda_{k,m,c}\times\left|\sum_{r=1}^{2}\mu_{k,r}^{(m)}\kappa_{k,c,r}^{(m)}\right|^2\right)\right]\right]\\&=E_{S\setminus\left\{\phi_{k,c,1}^{(m)}\right\}}\left[\exp\left(-\frac{\lambda_{k,m,c}}{4\sigma_B^2}\sum_{r=1}^{2}\left|\mu_{k,r}^{(m)}\kappa_{k,c,r}^{(m)}\right|^2\right)\times I_0\left(\frac{\lambda_{k,m,c}\upsilon_{k,c}^{(m)}}{2\sigma_B^2}\right)\right] \quad (30)\end{aligned}$$

where $\upsilon_{k,c}^{(m)}=|\mu_{k,1}^{(m)}||\kappa_{k,c,1}^{(m)}||\mu_{k,2}^{(m)}||\kappa_{k,c,2}^{(m)}|$ and $I_0(.)$ is the modified Bessel function of the first kind. Next, we condition over the remaining random variables except $\kappa_{k,c,1}^{(m)}$ and integrate over $\kappa_{k,c,1}^{(m)}$, where $\kappa_{k,c,1}^{(m)}\sim Rayleigh(\frac{\sigma^2_{\kappa,k,m,c,1}}{\sqrt{2}})$, as in (28), in which the equality (a) follows from [20, p. 294-Eq. 2.15.1.2] by noting that $\sum_{k=0}^{\infty}\frac{1}{k!}(\frac{c}{2\sqrt{p}})^{2k}=e^{c^2/4p}$ and setting $\nu=0$, $r=2$, $\alpha=2$, $c=\frac{\lambda_{k,m,c}|\mu_{k,1}^{(m)}||\mu_{k,2}^{(m)}||\kappa_{k,c,2}^{(m)}|}{2\sigma_B^2}$ and $p=(\frac{1}{\sigma^2_{\kappa,k,m,c,1}}+\frac{\lambda_{k,m,c}}{4\sigma_B^2}|\mu_{k,1}^{(m)}|^2)$. Now, we integrate over $\kappa_{k,c,2}^{(m)}$ where $\kappa_{k,c,2}^{(m)}\sim$ Rayleigh$(\frac{\sigma^2_{\kappa,k,m,c,2}}{\sqrt{2}})$.

$$\begin{aligned}&PEP_{k,m,c}\\&=E_{\left|\mu_{k,1}^{(m)}\right|,\left|\mu_{k,2}^{(m)}\right|}\left[E_{\left|\kappa_{k,c,2}^{(m)}\right|/\left|\mu_{k,1}^{(m)}\right|,\left|\mu_{k,2}^{(m)}\right|}[I_1]\right]\\&=E_{\left|\mu_{k,1}^{(m)}\right|,\left|\mu_{k,2}^{(m)}\right|}\left[\frac{4\sigma_B^2}{4\sigma_B^2+\lambda_{k,m,c}\sum_{r=1}^{2}\left|\mu_{k,r}^{(m)}\right|^2\sigma^2_{\kappa,k,m,c,r}}\right] \quad (31)\end{aligned}$$

From (31), we observe that the denominator contains a linear combination of two chi-squared random variables that may have different variances. Let $T_r=\sigma^2_{\kappa,k,m,c,r}|\mu_{k,r}^{(m)}|^2$. We can further write T_r in terms of a chi-square random variable with two degrees of freedom as $T_r=\frac{\sigma^2_{\kappa,k,m,c,r}\sigma^2_{\mu,k,m,r}}{2}Q_r$ where $Q_r\sim\chi_2^2$. Clearly, $T_r\sim Gamma(k_g=1,\theta_g=\sigma^2_{\kappa,k,m,c,r}\times\sigma^2_{\mu,k,m,r})$ where k_g and θ_g are respectively the shape and the scale parameters of the gamma distribution.

Let $Z=\sum_{r=1}^{2}|\mu_{k,r}^{(m)}|^2\sigma^2_{\kappa,k,m,c,r}=\sum_{r=1}^{2}T_r$. In case that

$$\sigma^2_{\kappa,k,m,c,1}\sigma^2_{\mu,k,m,1}=\sigma^2_{\kappa,k,m,c,2}\sigma^2_{\mu,k,m,2}, \quad (32)$$

then $Z\sim Gamma(k_g=2,\theta_g=\sigma^2_{\kappa,k,m,c,1}\sigma^2_{\mu,k,m,1})$. However, if $\sigma^2_{\kappa,k,m,c,1}\sigma^2_{\mu,k,m,1}\neq\sigma^2_{\kappa,k,m,c,2}\sigma^2_{\mu,k,m,2}$ and due to the structure of the matrix $\boldsymbol{U}_{k,m}$, one of the $\sigma^2_{\kappa,k,m,c,r}$ corresponding to the rth relay, $r\in\{1,2\}$, will be equal to zero. As a result, for this case $Z\sim Gamma(k_g=1,\theta_{g,nz}=\sigma^2_{\kappa,k,m,c,r_{nz}}\times\sigma^2_{\mu,k,m,r_{nz}})$ where r_{nz} is the index, r, of the nonzero

$$\begin{aligned}PEP_{k,m,c}&=E_{\left|\mu_{k,1}^{(m)}\right|,\left|\mu_{k,2}^{(m)}\right|,\left|\kappa_{k,c,2}^{(m)}\right|}\left[E_{\left|\kappa_{k,c,1}^{(m)}\right|/\left|\mu_{k,1}^{(m)}\right|,\left|\mu_{k,2}^{(m)}\right|,\left|\kappa_{k,c,2}^{(m)}\right|}\left[\exp\left(-\frac{\lambda_{k,m,c}}{4\sigma_B^2}\sum_{r=1}^{2}\left|\mu_{k,r}^{(m)}\kappa_{k,c,r}^{(m)}\right|^2\right)\times I_0\left(\frac{\lambda_{k,m,c}\left|\mu_{k,1}^{(m)}\right|\left|\kappa_{k,c,1}^{(m)}\right|\left|\mu_{k,2}^{(m)}\right|\left|\kappa_{k,c,2}^{(m)}\right|}{2\sigma_B^2}\right)\right]\right]\\&\overset{(a)}{=}E_{\left|\mu_{k,1}^{(m)}\right|,\left|\mu_{k,2}^{(m)}\right|,\left|\kappa_{k,c,2}^{(m)}\right|}\left[\underbrace{\frac{4\sigma_B^2}{4\sigma_B^2+\lambda_{k,m,c}\left|\mu_{k,1}^{(m)}\right|^2\sigma^2_{\kappa,k,m,c,1}}\exp\left(-\frac{\lambda_{k,m,c}\left|\mu_{k,2}^{(m)}\right|^2\left|\kappa_{k,c,2}^{(m)}\right|^2}{4\sigma_B^2+\lambda_{k,m,c}\left|\mu_{k,1}^{(m)}\right|^2\sigma^2_{\kappa,k,m,c,1}}\right)}_{I_1}\right] \quad (28)\end{aligned}$$

$\sigma^2_{\kappa,k,m,c,r}$ i.e., $r_{nz} = \{r | r \in \{1,2\}, \sigma^2_{\kappa,k,m,c,1}\sigma^2_{\mu,k,m,1} \neq \sigma^2_{\kappa,k,m,c,2}\sigma^2_{\mu,k,m,2}, \sigma^2_{\kappa,k,m,c,r_{nz}} \neq 0\}$. Therefore, in both cases, we can write the pdf of Z as $f_Z(z;k_g,\theta_g) = \frac{z^{k_g-1}e^{-z/\theta_g}}{\theta_g^{k_g}}$.

By integrating over Z, we get

$$
\begin{aligned}
&PEP_{k,m,c} \\
&= \int_0^\infty \frac{4\sigma_B^2}{4\sigma_B^2 + \lambda_{k,m,c} z} \frac{z^{k_g-1}}{\theta_g^{k_g}} \exp(-z/\theta_g) dz \\
&\overset{(a)}{=} \theta_g^{-k_g}(-1)^{k_g}\left(\frac{4\sigma_B^2}{\lambda_{k,m,c}}\right)^{k_g} \exp\left(\frac{4\sigma_B^2}{\lambda_{k,m,c}\theta_g^{k_g}}\right) Ei\left(-\frac{4\sigma_B^2}{\lambda_{k,m,c}\theta_g^{k_g}}\right) \\
&\quad - \sum_{p=1}^{k_g-1} (p-1)!(\theta_g)^{p-k_g}\left(-\frac{4\sigma_B^2}{\lambda_{k,m,c}}\right)^{k_g-p} \qquad (33)
\end{aligned}
$$

where the equality (a) follows from [21, p. 341-Eq. 3.353–5].

REFERENCES

[1] M. Stojanovic, "Underwater acoustic communications: Design considerations on the physical layer," in *Proc. 5th Annu. Conf. Wireless Demand Netw. Syst. Serv.*, Jan. 2008, pp. 1–10.

[2] L. Lu, T. Wang, S. C. Liew, and S. Zhang, "Implementation of physical-layer network coding," in *Proc. IEEE Int. Conf. Commun.*, Jun. 2012, pp. 4734–4740.

[3] F. Rossetto and M. Zorzi, "A practical architecture for OFDM-based decode-and-forward physical layer network coding," *IEEE Trans. Signal Process.*, vol. 60, no. 9, pp. 4747–4757, Sep. 2012.

[4] G. Bartoli, R. Fantacci, D. Marabissi, and R. Simoni, "Physical layer network coding in multipath channel: Effective precoding-based transmission scheme," in *Proc. IEEE Global Telecommun. Conf.*, Dec. 2011, pp. 1–5.

[5] Z. Li, X.-G. Xia, and B. Li, "Achieving full diversity and fast ML decoding via simple analog network coding for asynchronous two-way relay networks," *IEEE Trans. Commun.*, vol. 57, no. 12, pp. 3672– 3681, Dec. 2009.

[6] R. Vahidnia and S. ShabazPanahi, "Decentralized beamforming for multi-carrier asynchronous bi-directional relaying networks," in *Proc. IEEE ICASSP*, 2013, pp. 4202–4206.

[7] Y. Yao and X. Dong, "Optimal timing at the relay in OFDM based two way relay systems," *Wireless Pers. Commun.*, vol. 75, no. 2, pp. 1199–1213, Mar. 2014.

[8] Z. Wang, J. Huang, S. Zhou, and Z. Wang, "Iterative receiver processing for OFDM modulated physical-layer network coding in underwater acoustic channels," *IEEE Trans. Commun.*, vol. 61, no. 2, pp. 541–553, Feb. 2013.

[9] M. Rahmati and T. M. Duman, "Achieving delay diversity in asynchronous underwater acoustic (UWA) cooperative communication systems," *IEEE Trans. Wireless Commun.*, vol. 13, no. 3, pp. 1367–1379, Mar. 2014.

[10] N. Seshadri and J. Winters, "Two signaling schemes for improving the error performance of Frequency-Division-Duplex (FDD) transmission systems using transmitter antenna diversity," in *Proc. 43rd IEEE Veh. Technol. Conf.*, May 1993, pp. 508–511.

[11] S. Katti, S. Gollakota, and D. Katabi, "Embracing wireless interference: Analog network coding," *Wireless Netw.*, vol. 37, no. 4, pp. 397–408, Oct. 2007.

[12] V. Prathyusha, S. Bhashyam, and A. Thangaraj, "The Gaussian two-way diamond channel," in *Proc. 51st Annu. Allerton Conf. Commun., Control Comput.*, Oct. 2013, pp. 1292–1299.

[13] A. Salim and T. M. Duman, "An asynchronous two-way relay system with full delay diversity in time-varying multipath environments," in *Proc. ICNC*, Feb. 2015, pp. 900–904.

[14] Z. Wang and G. Giannakis, "Wireless multicarrier communications," *IEEE Signal Process. Mag.*, vol. 17, no. 3, pp. 29–48, May 2000.

[15] P. Schniter, "Low-complexity equalization of OFDM in doubly selective channels," *IEEE Trans. Signal Process.*, vol. 52, no. 4, pp. 1002–1011, Apr. 2004.

[16] B. Lu, X. Wang, and K. Narayanan, "LDPC-based space-time coded OFDM systems over correlated fading channels: performance analysis and receiver design," *IEEE Trans. Commun.*, vol. 50, no. 1, pp. 74–88, Jan. 2002.

[17] M. K. Park and V. Rodoplu, "UWAN-MAC: An energy-efficient MAC protocol for underwater acoustic wireless sensor networks," *IEEE J. Ocean. Eng.*, vol. 32, no. 3, pp. 710–720, Jul. 2007.

[18] D. Tse andP. Viswanath, *Fundamentals of Wireless Communication*. Cambridge, U.K.: Cambridge Univ. Press, 2005.

[19] P. Hou and W. Xu, "Super resolution time delay estimation for underwater acoustic sinusoidal signals," in *Proc. 2nd Int. Congr. Image Signal Process.*, Oct. 2009, pp. 1–6.

[20] A. Prudnikov, Y. A. Brychkov, and O. I. Marichev, *Integrals and Series*. New York, NY, USA: Gordon and Breach, 1986, vol. 2.

[21] I. Gradshteyn and I. Ryzhik, *Table of Integrals, Series, and Products*. Amsterdam, The Netherlands: Elsevier, 2007.

Ahmad Salim received the B.Sc. degree in electrical engineering from the University of Jordan, Amman, Jordan, in 2006 and the M.Sc. degree in telecommunication engineering from King Fahd University of Petroleum and Minerals, Dhahran, Saudi Arabia, in 2010. Currently, he is working towards the Ph.D. degree in electrical engineering at Arizona State University, Arizona, USA. He achieved eighth place in the University Qualifying Examination held in Jordan in the year 2005/2006 in the field of electrical engineering covering all the Jordanian universities. His primary research interests lie within the scope of communications and signal processing, including wireless communications, underwater acoustic communications, cooperative communications, MIMO systems, diversity techniques, error control coding and iterative receivers.

Tolga M. Duman (S'95–M'98–SM'03–F'11) received the B.S. degree from Bilkent University, Turkey, in 1993 and the M.S. and Ph.D. degrees from Northeastern University, Boston, MA, USA, in 1995 and 1998, respectively, all in electrical engineering. He is a Professor with the Electrical and Electronics Engineering Department, Bilkent University, Turkey, and is on leave from the School of ECEE at Arizona State University. Prior to joining Bilkent University in September 2012, he has been with the Electrical Engineering Department, Arizona State University, first as an Assistant Professor (1998–2004), then as an Associate Professor (2004–2008), and starting August 2008 as a Professor. His current research interests are in systems, with particular focus on communication and signal processing, including wireless and mobile communications, coding/modulation, coding for wireless communications, data storage systems and underwater acoustic communications.

Dr. Duman is a Fellow of IEEE, a recipient of the National Science Foundation CAREER Award and IEEE Third Millennium medal. He served as an editor for IEEE TRANSACTIONS ON WIRELESS COMMUNICATIONS (2003–08), IEEE TRANSACTIONS ON COMMUNICATIONS (2007–2012) and IEEE Communications Surveys and Tutorials (2002–07). He is currently the coding and communication theory area editor for IEEE TRANSACTIONS ON COMMUNICATIONS (2011–present) and an editor for *Elsevier Physical Communications Journal* (2010–present).